Two Stable Equilibria of a Coupled Ocean–Atmosphere Model

S. MANABE AND R. J. STOUFFER

Geophysical Fluid Dynamics Laboratory/NOAA, Princeton University, Princeton, New Jersey

(Manuscript received 1 September 1987, in final form 4 May 1988)

ABSTRACT

Two stable equilibria have been obtained from a global model of the coupled ocean–atmosphere system developed at the Geophysical Fluid Dynamics Laboratory of NOAA. The model used for this study consists of general circulation models of the atmosphere and the world oceans and a simple model of land surface. Starting from two different initial conditions, "asynchronous" time integrations of the coupled model, under identical boundary conditions, lead to two stable equilibria. In one equilibrium, the North Atlantic Ocean has a vigorous thermohaline circulation and relatively saline and warm surface water. In the other equilibrium, there is no thermohaline circulation, and an intense halocline exists in the surface layer at high latitudes. In both integrations, the air–sea exchange of water is adjusted to remove a systematic bias of the model that surpresses the thermohaline circulation in the North Atlantic. Nevertheless, these results raise the intriguing possibility that the coupled system may have at least two equilibria. They also suggest that the thermohaline overturning in the North Atlantic is mainly responsible for making the surface salinity of the northern North Atlantic higher than that of the northern North Pacific. Finally, a discussion is made on the paleoclimatic implications of these results for the large and abrupt transition between the Alleröd and Younger Dryas events which occurred about 11 000 years ago.

1. Introduction

Based upon the results from highly idealized models of thermohaline circulation, Stommel (1961) and Rooth (1982) have suggested that the oceans may possess more than one stable equilibria. By use of a general circulation model of an ocean with an idealized sector geography, F. Bryan (1986) demonstrated that an equationally asymmetric circulation can be maintained even with an equatorially symmetric geography and surface forcing. He noted that the system has at least three equilibrium solutions for the same forcing: an equatorially symmetric circulation, and two mirror-image, pole-to-pole circulations. Although he did not identify it as such, his model appears to have yet another solution which is characterized by the development of an intense halocline in high latitudes of both hemispheres and the absence of deep water formation and thermohaline circulation.

The climatic record obtained from the long Greenland ice core reveals several climatic oscillations which may be caused by fluctuations in the rate of formation of deep water. Based upon this and other geological evidence, Oeschger et al. (1984) and Broecker et al. (1985) suggested that the oceans have more than one stable mode of thermohaline circulation.

This paper describes two stable equilibria obtained from the time-integrations of a global coupled ocean-atmosphere model, which were conducted under identical boundary conditions but originated from two different initial conditions. In one of these equilibria, an interhemispheric thermohaline circulation is maintained in the North Atlantic Ocean, whereas, in another equilibrium, it is absent. The former has warmer and more saline surface water in high latitude regions of the North Atlantic Ocean and is more realistic than the latter. The main objectives of the present study are the exploration of the mechanisms which are responsible for these bistable equilibria and the assessment of their geophysical relevance.

The double equilibria were discovered inadvertently in the course of the study of climate sensitivity to CO_2 forcing. In this study, it was necessary to adjust the rate of water exchange at the ocean–atmosphere interface in order to remove a systematic bias of the model. In view of this artificial adjustment of surface water flux, one has to regard the present results with caution. Nevertheless, it was decided to publish the present results for the following reasons. First, a detailed analysis of the mechanisms involved in maintaining the two equilibria persuaded the authors of the plausibility of their existence. Second, an intercomparison between the two equilibria with and without the North Atlantic thermohaline circulation is very useful for identifying the role of this circulation in maintaining the observed water mass structure of the Atlantic Ocean.

The present paper begins with the description of the coupled ocean–atmosphere model, followed by an ex-

Corresponding author address: Dr. S. Manabe, NOAA/GFDL, Princeton University, P.O. Box 308, Princeton, NJ 08542.

planation of the procedures through which the double equilibria were obtained. It then describes the bistable equilibria and discusses the mechanisms which maintain them. Finally, the study evaluates the relevance of the present result to the drastic transition of climate from the Alleröd to Younger Dryas stades. The concluding section of the paper contains an overall assessment of the present results and the discussion of their geophysical significance.

2. The coupled model

a. Model structure

The coupled ocean–atmosphere model used for this study consists of a general circulation model of the world oceans coupled to a general circulation model of the atmosphere with the heat and water budgets of the continental surface. It has a global domain, a realistic geography, and annually averaged insolation. Figure 1 is a box diagram which illustrates the basic components of the model and the interaction among them. The remainder of this subsection describes the details of the model structure and may be skipped in the preliminary reading.

In the atmospheric component of the model the dynamic computation is performed using a semispectral method in which the horizontal distribution of the predicted variable is represented by a truncated series of spherical harmonics and grid point values (Gordon and Stern 1982). The resolution is limited by a cutoff beyond a zonal wavenumber of 15. The same degrees of freedom are permitted in representing the latitudinal distribution of each zonal wave component. The effects of clouds, water vapor, carbon dioxide, and ozone are included in the calculation of solar and terrestrial radiation. The distribution of water vapor is predicted

in the model, but the mixing ratio of carbon dioxide is assumed to be a constant in the model atmosphere. Ozone is specified as a function of latitude and height from observations. The annually averaged values of height, thickness and fractional amount of cloud cover are also specified by use of the results of London (1957) and Sasamori et al. (1972). Another major simplification of the model is the specification of solar radiation without seasonal variation. The solar constant is assumed to be 1353 W m^{-2}.

Precipitation is simulated whenever supersaturation is indicated by the prognostic equation for water vapor. It is identified as snowfall when the air temperature near the surface falls below freezing; otherwise it is identified as rain. Moist convective processes are parameterized by a moist convective adjustment scheme as described in Manabe et al. (1965).

The land surface temperature is determined in such a way that it satisfies the constraint of no surface heat storage. That is, the contributions from net fluxes of solar and terrestrial radiation and turbulent fluxes of sensible and latent heat must balance locally. The albedo distribution of snow-free surfaces is determined by referring to the study of Posey and Clapp (1964). When the surface is covered by snow, the albedo is replaced by a higher value depending on surface temperature and snow depth. For deep snow (water equivalent at least 2 cm), the surface albedo is 60% if the surface temperature is below $-10°C$ and 45% at $0°C$, with a linear interpolation between these values from $-10°C$ to $0°C$. When the water equivalent of the snow depth is less than 2 cm, it is assumed that the albedo decreases from the deep snow values to the albedo of the underlying surface as a square root function of snow depth.

The change in snow depth is computed as the net contribution of snowfall, sublimation, and snowmelt
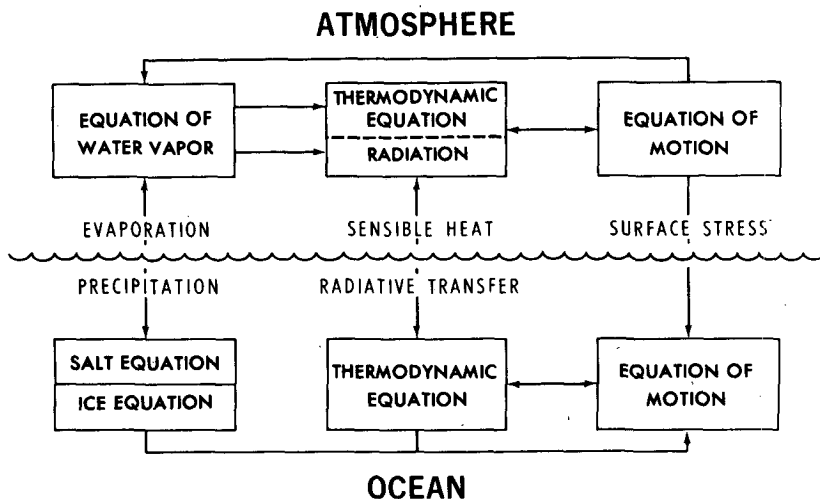

FIG. 1. Box diagram which identifies the major components of the coupled ocean-atmosphere model and their interactions.

which is determined from the requirement of surface heat balance (see Manabe 1969 for further details).

The budget of soil moisture is computed by the so-called bucket method. Within the model, soil is assumed to have the ability to contain 15 cm of liquid water. (This is known as the "field capacity.") When soil is not saturated with water, the change of soil moisture is predicted as a net contribution of rainfall, evaporation, and snowmelt. If the soil moisture value reaches the field capacity, the excess water is regarded as runoff. The rate of evaporation from the soil surface is determined as a function of the water content of the "bucket" and potential evaporation, i.e., the hypothetical evaporation rate from a completely wet surface.

The oceanic component of the model is similar to the model described by Bryan and Lewis (1979). The so-called primitive equations of motion are constructed by use of Boussinesq, rigid lid, and hydrostatic approximations. It represents subgrid scale turbulent viscosity as enhanced molecular mixing. The prognostic equations of temperature and salinity contain the contributions from advection and subgrid scale diffusion. Whenever the vertical stratification in model oceans is unstable, it is assumed that the coefficient of vertical diffusion becomes infinitely large, and the vertical gradients of both temperature and salinity are removed. This process of convective adjustment together with the large-scale sinking of dense water contributes to the formation of deep water in the model oceans.

The finite difference mesh of the oceanic component of the model has a spacing between grid points of 4.5° longitude and 3.75° latitude. It has 12 levels for the finite differencing in the vertical direction. The computational resolution specified above is marginally adequate for representing coastal currents but cannot describe mesoscale eddies.

The bathymetry of the model is shown in Fig. 2. Because of the coarse computational resolution, many features of bottom topography are crudely resolved. For example, the mid-Atlantic Ridge of the model is not as tall as observed and Iceland is eliminated. No attempt is made to resolve the flow through the Strait of Gibraltar. Instead, the water at the westernmost Mediterranean grid point is mixed horizontally and completely with the water at the adjacent Atlantic grid point to a depth of 1350 m.

The prognostic system of sea ice is similar to the very simple system developed by Bryan (1969). The sea ice drifts with the surface ocean currents provided that its thickness is less than 4 m, but is stationary for higher value. As developed by Broccoli and Manabe (1987), the albedo of sea ice depends on surface temperature and ice thickness. For thick sea ice (at least 1 m thick), the surface albedo is 80% if the surface temperature is below −10°C and 55% at 0°C, with a linear interpolation between these values for intermediate temperatures. If the ice thickness is less than 1 m, the albedo decreases from the thick ice values to the albedo of the underlying water surface as a square root function of ice thickness.

As indicated in Fig. 2.1, the atmospheric and oceanic components interact with each other through exchanges of heat, water, and momentum. The heat exchange is accomplished by the net radiative flux and turbulent fluxes of sensible and latent heat. The water (or ice) exchange consists of evaporation (or sublimation), rainfall (or snowfall), and runoff from the continents. The rate of runoff is computed by assuming that water flows towards the direction of the steepest orographic gradient. Glacier flow is computed in a similar manner. In order to prevent indefinite growth of the ice sheet through snow accumulation, it is assumed that the ice thickness does not exceed 20 cm and the excess snow runs off to the direction of the steepest descent and instantly reaches the oceans. The ocean surface temperature and sea ice predicted in the ocean are used as lower boundary conditions for the atmosphere. Details of the heat, moisture, and momentum exchange processes are given, for example, by Manabe (1969).

b. Asynchronous integration

The heat capacity of the entire atmosphere is less than the heat capacity of the upper 2 m of the ocean. This is why the response time of the atmosphere alone to climate forcing is relatively short, while the equilibration time of the coupled ocean–atmosphere system is of the order of centuries. Seeking climate equilibrium of a coupled ocean–atmosphere system through a direct numerical integration with respect to time is impractical. Such an integration would have to resolve both the high frequencies related to synoptic systems in the atmosphere, as well as ultralow frequencies related to the water mass adjustment in the deep ocean. As an alternative we seek a balanced thermal state through asynchronous time-integration in which the atmospheric and oceanic components of the model are integrated concurrently over two different periods (Manabe and Bryan 1969; Manabe 1969). In each experiment, the atmospheric component is integrated for 8.2 years. At the same time, the ocean is integrated for 1250 years, continuously exchanging the boundary conditions with the atmosphere. The approach of deeper ocean layers towards equilibrium is accelerated further by reducing the effective heat capacity of water as described by Bryan et al. (1975) and Bryan (1984), extending the effective period of integration to 34 000 years. No systematic drift of the final equilibrium state of the coupled system occurs near the end of each time integration.

3. Numerical experiments

Figure 3 illustrates the sequences of several numerical time integrations from which the two stable equi-
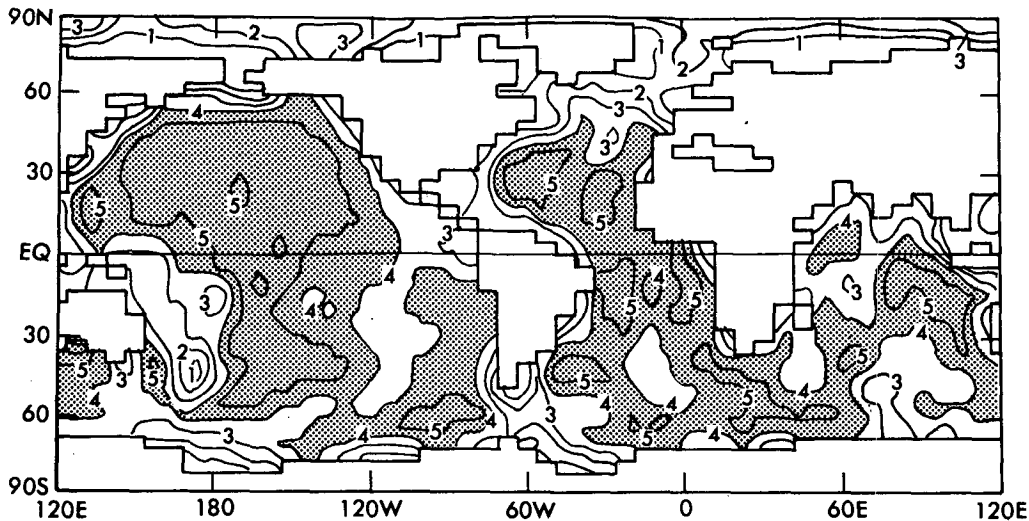
FIG. 2. The topography of the ocean model. Depths are given in kilometers.

libria were obtained. This section explains how these experiments were conducted and describes the results obtained from them.

a. Preliminary experiment

The coupled model is time-integrated from an isothermal and dry atmosphere at rest coupled with an isothermal ocean at rest and with uniform salinity. For economy of computation the asynchronous method described in section 2b is used. Towards the end of this preliminary experiment, there is no systematic trend in the temporal variability of the model climate.

Figure 4 compares the geographical distributions of time-mean sea surface temperatures obtained from the last stage of the preliminary experiment with the observed distribution. Although the simulated distribution resembles the observed, there are many differences between them. In particular, the simulated sea surface temperature over the northern North Atlantic is significantly lower than the observed. This underestimation results from the absence of the thermohaline circulation which advects warm surface water northwards from low latitudes.

The geographical distribution of surface salinity from the preliminary experiment is compared with the ob-
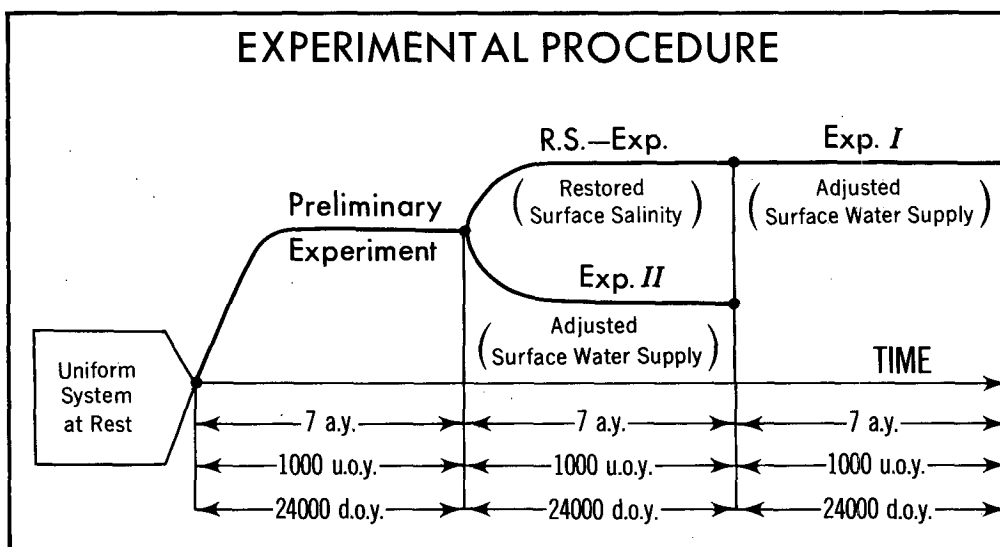

FIG. 3. Diagram which illustrates the succession of experiments conducted in the present study. For the description of the experiments, see the main text. The abbreviations a.y., u.o.y., and d.o.y. in the bottom of the figure represent atmospheric years, upper ocean years, and deep ocean years, respectively.
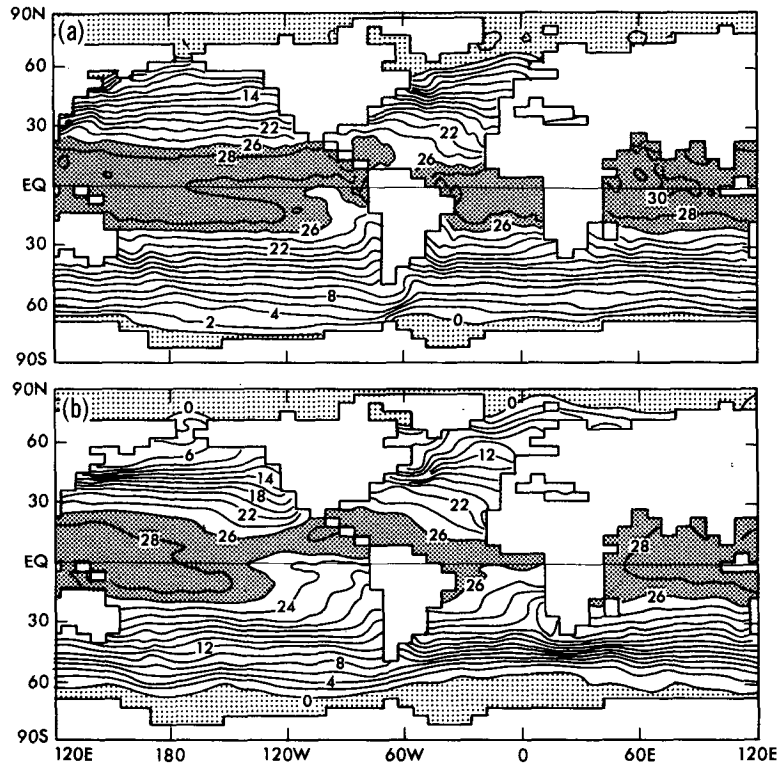
FIG. 4. (a) Time mean sea surface temperature (°C) from the preliminary experiment.
The time averaging was performed over the last 500 upper ocean years of the model.
(b) Observed sea surface temperature (degrees Celsius) (Levitus 1982).

served distribution in Fig. 5. Again, because of the absence of thermohaline overturning, northward advection of saline surface water from low latitudes does not occur in the North Atlantic. Thus, the North Atlantic surface salinity is very low and is substantially below the simulated salinity in the North Pacific in sharp disagreement with the observed distribution. As discussed below, the intense halocline in the northern North Atlantic prevents thermohaline overturning in the Atlantic Ocean in this preliminary experiment.

b. RS-experiment

The results from the preliminary experiments described above indicate that the coupled model failed to simulate some of the basic characteristics of ocean circulation and water mass in the North Atlantic Ocean. Such a model can yield unreliable results when it is used for studies of sensitivity and variability of climate. For example, the albedo feedback process of a model may be distorted if the distributions of sea water temperature and sea ice margin are unrealistic as indicated in the results from the basic experiment. Or, the absence of the thermohaline circulation in the North Atlantic Ocean of the model may result in the underestimation of the downward penetration of the

warm anomaly which occurs in response to the increase of greenhouse gases in the atmosphere. Therefore, further improvement of the model is required before one can use it with confidence for the study of climatic change.

As a stop gap measure, one could impose an external forcing which counter-balances the bias of the model, thereby making its behavior more realistic. In view of the particularly poor performance of the model in reproducing the observed distribution of surface salinity in the North Atlantic, it was decided to continuously adjust the supply of water at the surface of the model oceans such that a realistic distribution of surface salinity is maintained throughout each time integration to counterbalance the bias of the model. In order to determine the required adjustment of surface water supply, the coupled model is time-integrated while continuously restoring the surface salinity to its observed annual mean distribution with a time constant of 30 days. The initial condition for this integration, which will be identified in Fig. 3 as the RS-experiment, is the state reached at the end of the preliminary experiment described in the preceding subsection. Although the North Atlantic thermohaline circulation is absent at first, it appears as the integration proceeds. In the final stage of this RS-experiment, the temporal
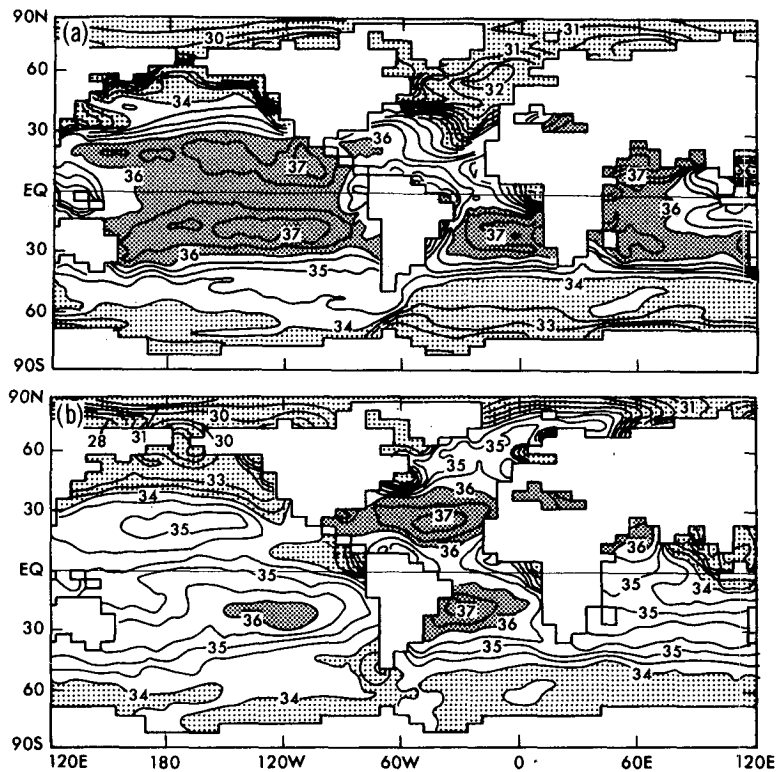
FIG. 5. (a) Time mean sea surface salinity (‰) from the preliminary experiment. The time averaging was performed over the last 500 upper ocean years of the model. (b) Observed surface salinity (‰) (Levitus 1982).

atic trend. During this final stage, the surface water flux required for restoring the observed surface salinity is computed and time-averaged. Because of the bias of the model, this flux differs substantially from the surface water flux, which is computed internally by the model as the difference between the sum of precipitation and runoff minus evaporation. The geographical distribution of the time-mean difference between these two fluxes is described in the Appendix. Throughout the two time integrations described in subsection 3c below, the surface water flux of the model is adjusted by an amount equal to this difference to counterbalance the model bias.

c. Experiments I and II

Starting from the state attained at the end of the RS-experiment, the coupled model is time-integrated asynchronously with the adjustment of the surface water supply as described above. Although the surface salinity is no longer restored to the observed distribution during this integration, it nevertheless remains near the observed values owing to the water flux adjustment. In contrast to the results from the preliminary experiment, a thermohaline circulation of significant intensity is sustained in the Atlantic Ocean, thereby maintaining a realistically high level of surface salinity in
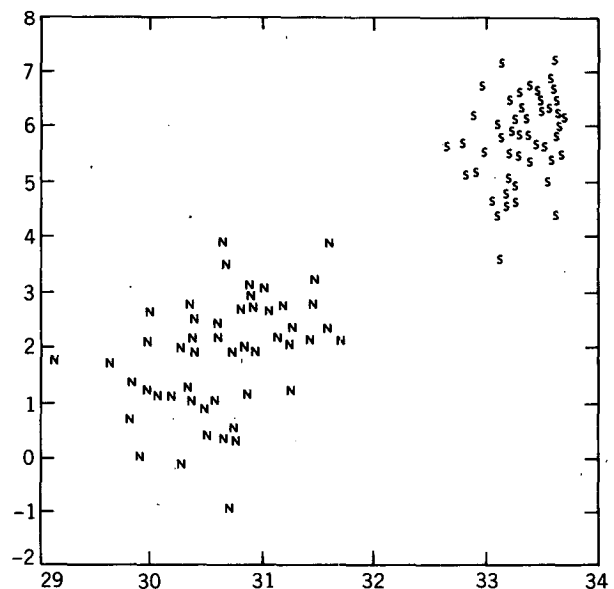

FIG. 6. The scatter plots represent the instantaneous temperature and salinity of surface water averaged over the zonal belt of the northern North Atlantic located between 50° and 70°N latitudes. The ordinate and abscissa of the figure denote temperature (degrees Celsius) and salinity (ppt), respectively. The letters S and N indicate the results from experiments I and II, respectively. The sampling period for this analysis is the last 500 upper ocean years from each asynchronous time integration.

the northern North Atlantic through the northward advection of saline surface water from low latitudes.

On the other hand, when the time integration started from the state reached at the end of the preliminary (rather than RS-) experiment, it led to a state characterized by low salinity surface water and no Atlantic thermohaline circulation despite the adjustment of water flux described above. In short, two integrations of an identical model with an identical water flux adjustment generate two stable equilibria depending upon whether the initial condition has a thermohaline circulation in the North Atlantic Ocean or not. These two experiments, with and without thermohaline circula-

tion, are identified as experiments I and II, respectively. Figure 3 indicates the chronologies of the two experiments.

Figure 6 shows that the two equilibria from these two asynchronous integrations are stable and distinct from each other. Each plot represents the instantaneous area mean values of surface temperature and surface salinity in the zonal belt of the North Atlantic located between 50° and 70° latitudes. The points S and N represent values from the first and second asynchronous integrations, respectively. All S-points are located around the point with temperatures of 6°C and salinity of 33.3‰. The N-points scatter around lower values
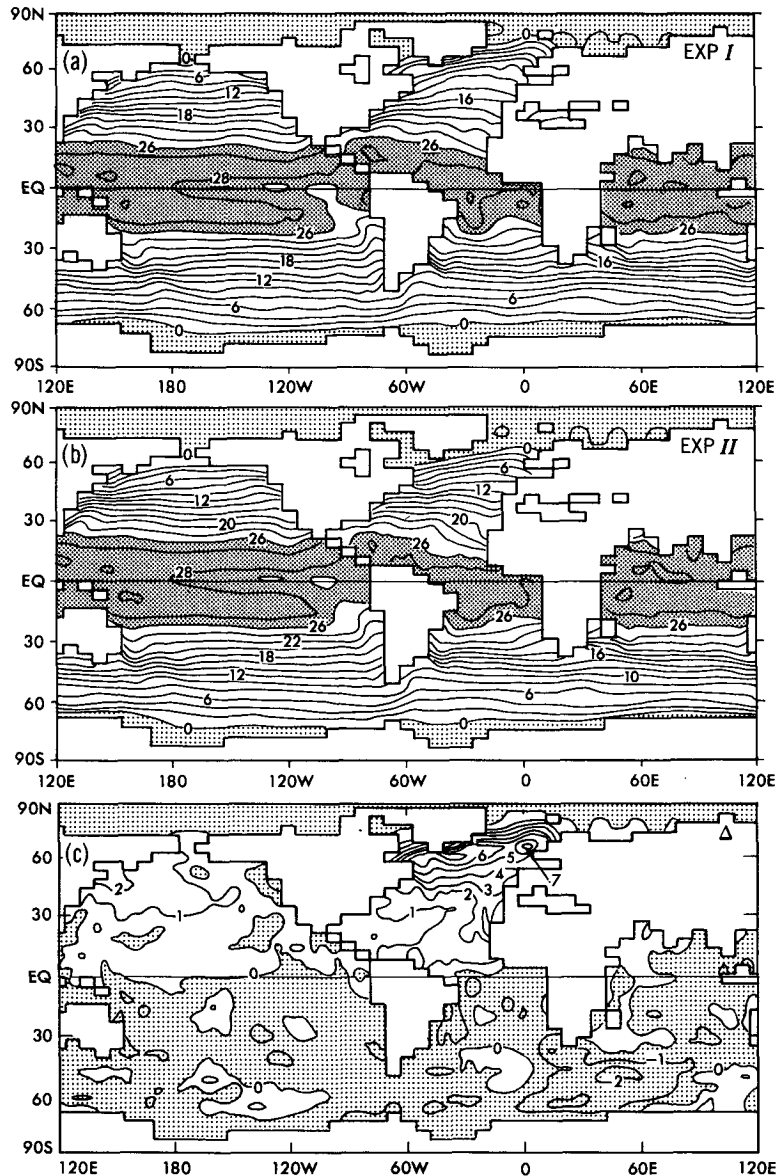

FIG. 7. (a) Sea surface temperature (degrees Celsius) from experiment I. (b) Sea surface temperature (degrees Celsius) from experiment II. (c) The difference (degrees Celsius) between the two sea surface temperatures (i.e., (a) minus (b)).

of temperature and salinity, i.e., 2°C and 30.7‰, respectively. The analysis period covers the last 500 upper ocean years of each asynchronous integration. Most importantly, the domain occupied by the N-points does not overlap the S-domain suggesting that the two North Atlantic water mass structures from experiments I and II are distinct.

4. Double equilibria

This section compares the structure of the two stable equilibria obtained from experiments I and II, and ex-

plores the processes which maintain them. Each equilibrium is determined by averaging over the last 5 atmospheric years, 500 upper ocean years or 40 000 deep ocean years of the asynchronous time integrations.

a. Water mass characteristics

Figure 7 contains the horizontal distributions of the ocean surface water temperature from experiment I and II, and their difference (I minus II). The two equilibria differ significantly from each other over the North Atlantic Ocean where experiment I is warmer than ex-
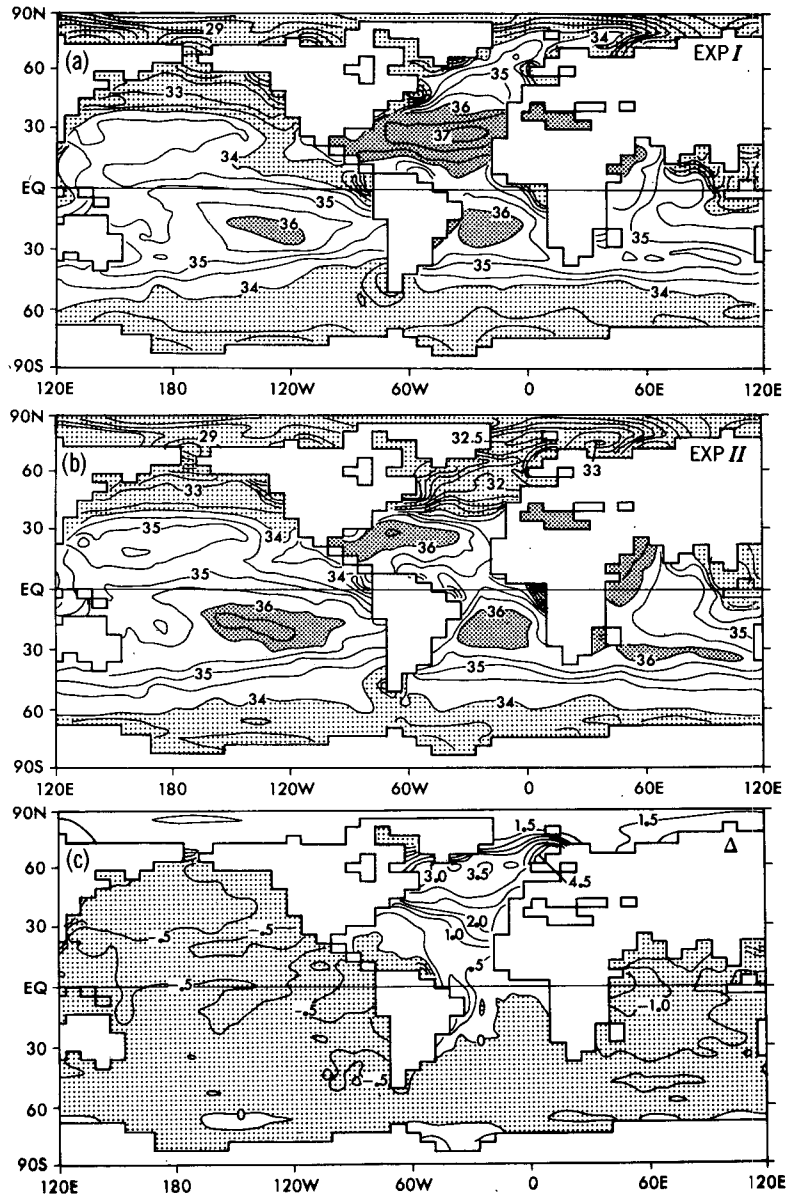

FIG. 8. (a) Sea surface salinity (ppt) from experiment I. (b) Sea surface salinity (ppt) from experiment II. (c) The difference (ppt) between the two sea surface salinity [i.e., (a) minus (b)].
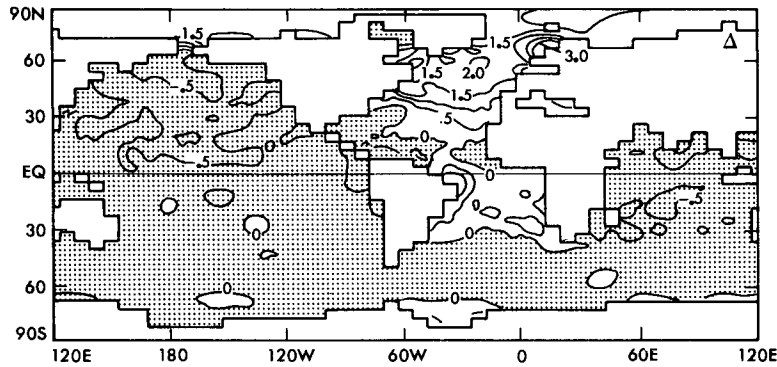
FIG. 9. The difference in surface water density (ppt) between experiments I and II.

periment II (Figs. 7a and 7b). Figure 7c shows that the difference is most pronounced poleward of 40°N. The northward advection by the thermohaline circulation helps maintain the warm surface water over the North Atlantic in experiment I, whereas such a circulation is missing in experiment II. In the rest of the Northern Hemisphere the difference in surface temperature is small but positive. In the Southern Hemisphere, experiment I is slightly cooler than experiment II. The zonal advection of the Atlantic thermal anomalies by the atmospheric circulation may be partly responsible

for the small positive difference in the Pacific Ocean of the Northern Hemisphere. The reduction of the equatorward ocean surface Ekman drift due to the weakening of surface westerlies may also contribute to this positive difference.

The distributions of surface salinity from the two experiments and the difference between them are shown in Fig. 8. Experiment I is saltier than experiment II in the North Atlantic Ocean. The difference is particularly large around 55°N reaching a value of 3.5‰. As discussed later, the northward advection of saline
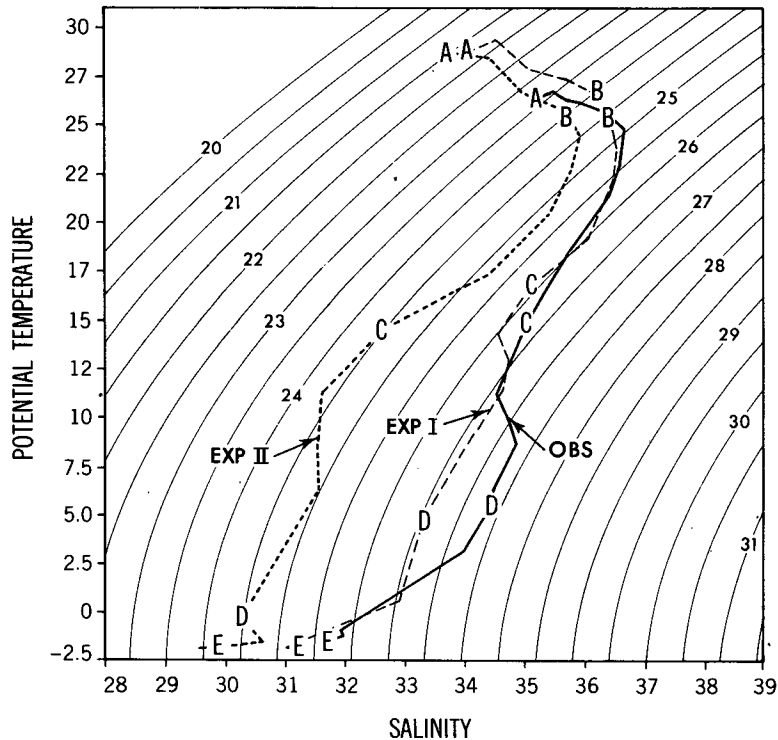

FIG. 10. Temperature–salinity (T–S) diagram of the zonal mean properties of surface water at the selected latitudes of the Atlantic Ocean (A: 2.2°N, B: 20°N, C: 42.2°N, D: 64.4°N, E: 87.3°N). Dashed line: experiment I. Dotted line: experiment II. Solid line: observed.

water by the thermohaline circulation is again responsible for maintaining the relatively high surface salinity over the North Atlantic Ocean in experiment I. The difference in the rest of the world oceans is small but negative. The distribution of surface salinity from experiment I is much more realistic than the distribution from experiment II (compare Figs. 8a and 8b with Fig. 5b). In qualitative agreement with the features of the actual ocean, the surface salinity of the North Atlantic is much higher than that of the North Pacific in experiment I. The opposite is the case for experiment II, underscoring the large influence of the thermohaline circulation in determining surface salinity.

The distribution of surface density is computed from the distributions of surface temperature and salinity described above. Fig. 9 illustrates the geographical distribution of the difference in surface density between experiments I and II. Over the North Atlantic Ocean, the surface density from experiment I is larger than the corresponding density from experiment II. The difference between the two experiments is more than 2.0 $\times$ 10^{-3} g cm^{-3} at about 50°N, but it is almost zero in the equatorial Atlantic. Thus, the meridional gradient of surface density in experiment I is larger than experiment II in the North Atlantic Ocean.

To compare the simulated latitudinal distributions of zonal mean surface temperature, salinity and density from the two experiments with the observed distributions over the North Atlantic Ocean, the T-S diagram in Fig. 10 is constructed. Over the North Atlantic the latitudinal distributions of salinity and temperature from experiment I are in good agreement with the observed profiles. On the other hand, the surface water in the northern North Atlantic is too fresh and too cold and its density is too small in experiment II. The density is unrealistically small in experiment II despite its low temperature because of the low salinity. (As this T-S diagram indicates, the density of surface water depends little upon temperature near the freezing point.) In summary, over northern North Atlantic, the zonal mean surface density in experiment I is realistic and is much larger than the corresponding density in experiment II, thereby inducing sinking and the thermohaline circulation as discussed later.

The water mass characteristics from the two experiments are also different in the deeper layers of the model oceans. Figure 11a shows the latitude–depth distribution of the difference in the zonally averaged temperature in the Atlantic Ocean. The surface temperature difference is at a maximum at about 60°N (see also Fig. 7c). This positive anomaly penetrates downward and southward in the deep layers of the Atlantic Ocean. The negative anomaly is at a maximum in the Southern Hemisphere near 20°S at a depth of 2500 meters.

Fig. 11b is a latitude vs depth representation of the difference in salinity in the Atlantic Ocean. The surface salinity maximum is located at about 60°N. In qualitative agreement with the temperature difference, the

difference in surface salinity is at a maximum at high latitudes of the Atlantic Ocean. Again, the positive anomaly penetrates downward and extends southward in the deep layers of the Atlantic Ocean.

Because of the compensation between the temperature and salinity anomalies, the zonal mean density difference between experiments I and II is small in most of the deep layers of the Atlantic Ocean as indicated in Fig. 11c. This suggests that in experiment I with the thermohaline circulation the southward flow of water
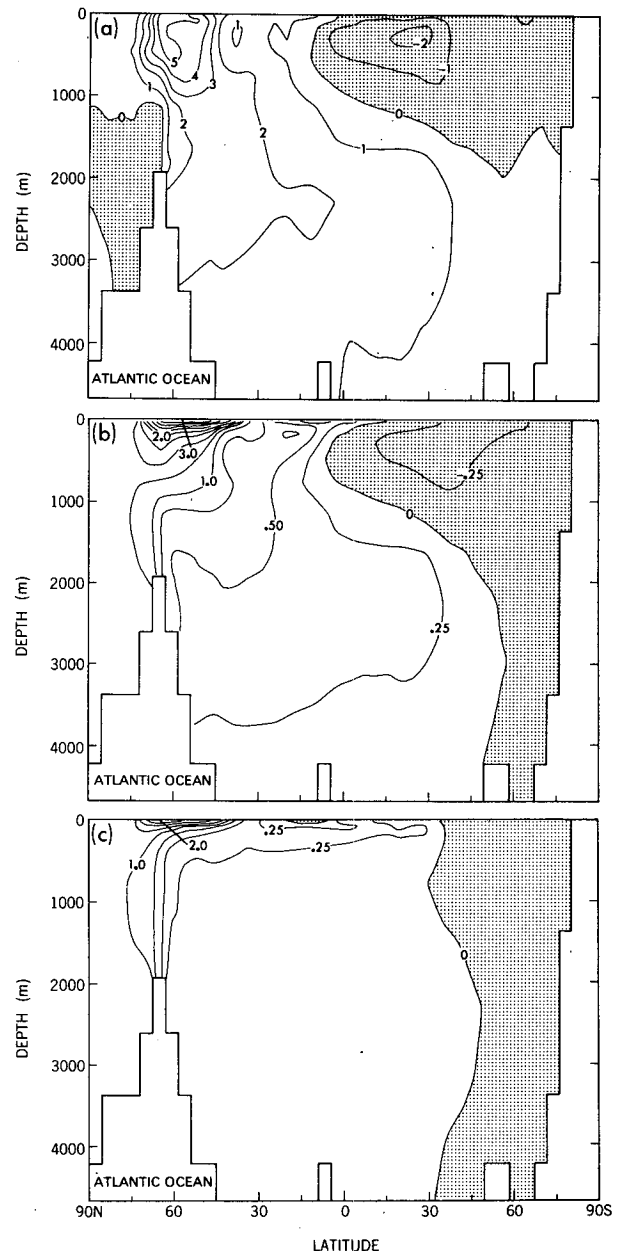

FIG. 11. The latitude–depth distribution of the difference in water properties zonally averaged in the Atlantic Ocean. (a) Temperature difference (degrees Celsius), (b) salinity difference (ppt), and (c) density difference in σ_t.

in the deep layer of the Atlantic Ocean occurs along isopycnal surfaces. However, a large positive density difference is indicated in the surface layer of the ocean polewards of 45°N. It extends downward at very high latitudes where strong convective activity prevails. These positive density differences account for the difference in thermohaline circulation between the two experiments as described in subsection 4b below.

b. Thermohaline circulation

Figures 12a and 12b display the streamfunction of the meridional circulation in the Atlantic Ocean from experiments I and II. In experiment I, water flows northward in the upper layer of the Atlantic Ocean

and returns southward below a depth of 1 km. The total mass transport involved in this Atlantic circulation is approximately 12 Sv (1 Sv $\equiv 10^6$ m^3 s^{-1}). This is about $2/3$ of the actual overturning transport estimated by Bryden and Hall (1980) at 25°N. However, in experiment II there is no thermohaline circulation of significant magnitude in the North Atlantic as illustrated by Fig. 12b.

As discussed already, this difference in thermohaline circulation between the two experiments accounts for the basic features of temperature and salinity differences described in subsection 4a. Because of the advection of temperature and salinity by the northward flow in the top layer of the Atlantic Ocean of the model, both surface temperature and salinity in experiment I
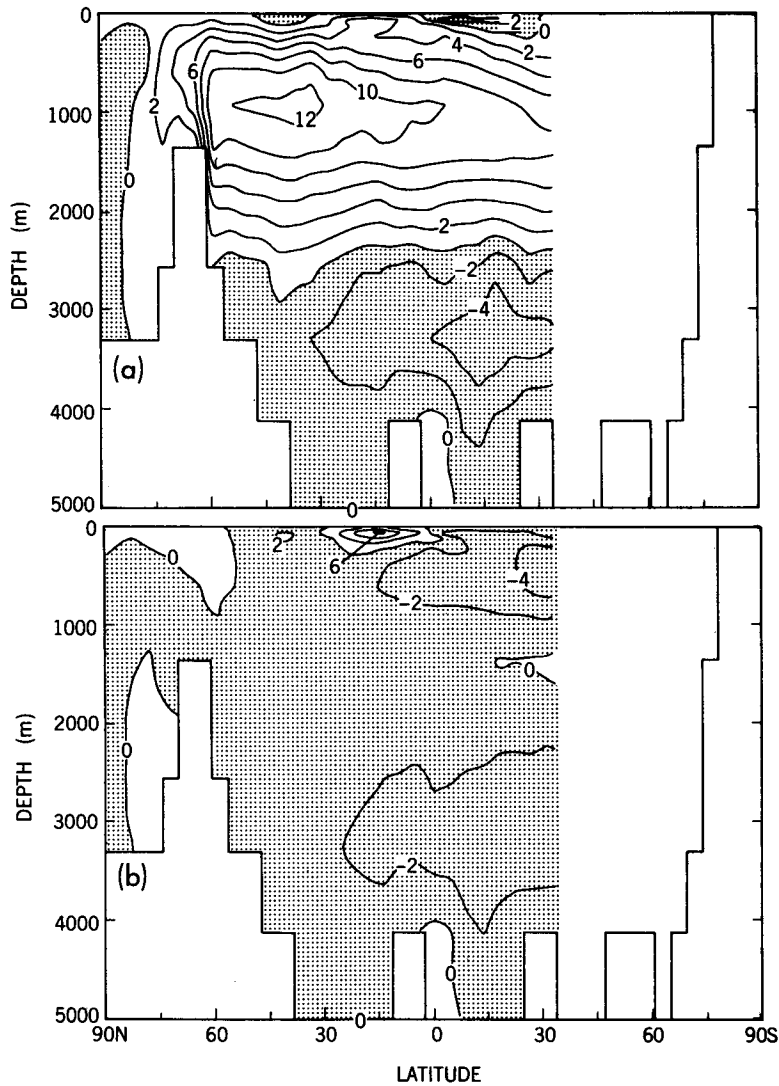

FIG. 12. Streamfunction illustrating meridional circulation in the Atlantic Ocean. Units are in Sverdrups (i.e., 10^6 m^3 s^{-1}). (a) Experiment I. (b) Experiment II. The streamfunction is not shown in the southern Atlantic which is not enclosed by coastal boundaries and freely exchanges water with other oceans.

are larger than those in experiment II in the Northern Hemisphere, particularly in high latitudes. Advection by the thermohaline circulation is also responsible for the downward and southward extensions of the positive anomalies of both temperature and salinity from the subarctic region. In the Southern Hemisphere, the meridional gradients of surface temperature and salinity reverse sign from the Northern Hemisphere, and the advection of these variables by the northward flow also reverse sign. Therefore, the differences in both surface temperature and salinity between the two experiments are negative and are opposite from the Northern Hemisphere in the Atlantic Ocean as indicated in Figs. 7c and 8c.

It is reasonable to expect that the difference in the meridional circulations of the two equilibria manifests itself in the horizontal components of the ocean currents. Figures 13a and 13b illustrate the distributions of surface current vectors from experiments I and II, respectively. The differences in the surface flow fields between the two experiments are pronounced in the North Atlantic Ocean. In the flow field from experiment I with the thermohaline circulation, part of the Gulf Stream separates from the subtropical gyre and flows into the Norwegian Sea. The flow field from experiment II without the North Atlantic thermohaline circulation is quite different. Part of the surface current flows southward along the coast of Newfoundland and joins the subtropical gyre. The flow field from experiment I resembles the observed flow in the North At-

lantic, whereas the surface flow from experiment II resembles the surface circulation in the northern Pacific where the thermohaline circulation is very weak. (In the South Atlantic, the Benguela current along the west coast of Africa heads southward in both experiments in disagreement with observation.)

The difference in surface currents in the North Atlantic accounts for the differences in the distributions of surface salinity in middle and high latitudes. In experiment I, the penetration of surface currents from the coastal region of North America all the way to the coast of northern Europe is responsible for the northward penetration of the positive salinity anomaly at the surface. In experiment II, southward currents from the coast of Newfoundland to the west coast of North Africa extends the region of low surface salinity into middle and subtropical latitudes.

Figures 14a and 14b illustrate the difference in the flow field between the two experiments at the surface and 1622 m depth. The difference currents pass the Cape of Good Hope, go westwards across the South Atlantic Ocean, and reach the east coast of South America. They flow northwards along the coast of South and North America, and finally turn eastward reaching the west coast of northern Europe. In deep water, the difference currents flow in the opposite direction along the same route. The difference currents at the surface and at 1622 m depth clearly indicate the path of the thermohaline circulation in the Atlantic Ocean of the model.
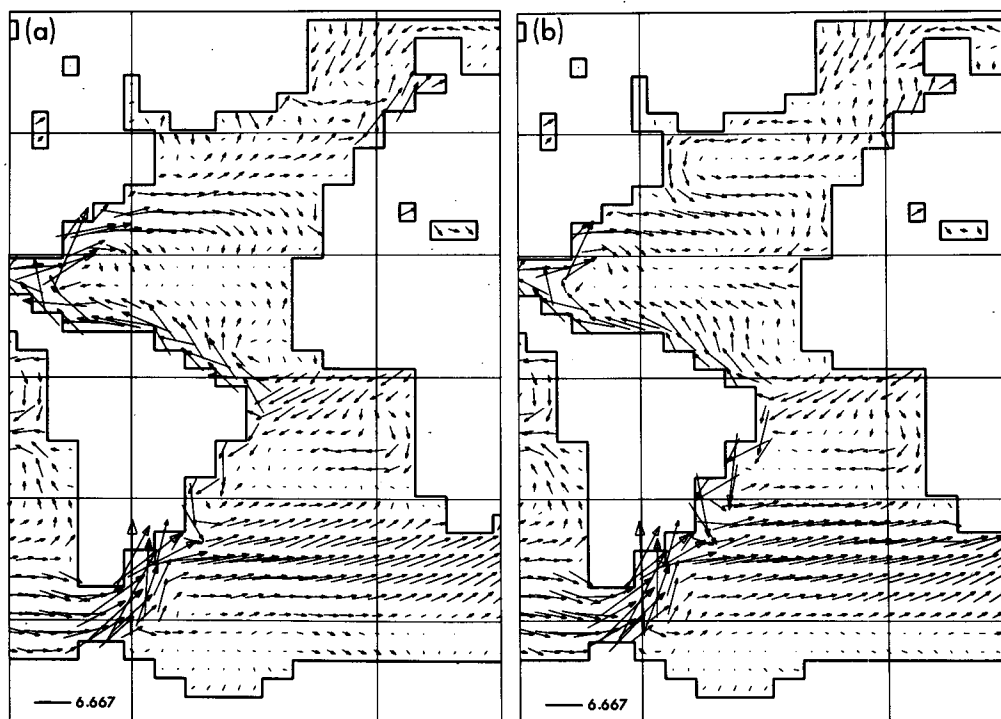

FIG. 13. Vectors of surface ocean currents in the Atlantic sector. (a) Experiment I. (b) Experiment II.
See the lower left corners of each map for scaling in units of centimeters per second.
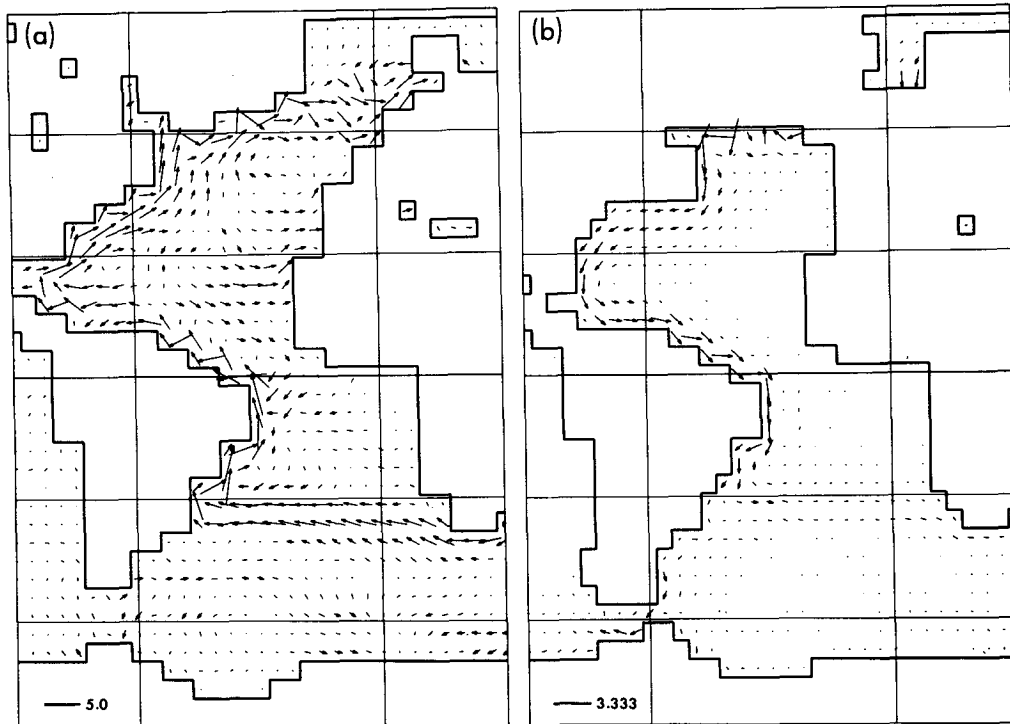
FIG. 14. Vectors indicating the difference in ocean currents between experiments I and II at (a) the surface, and (b) a depth of 1622 m. See the lower left corners of each map for scaling. Here, units are in centimeters per second.

Although it is not shown here, the surface currents which flow around the southern tip of Africa originate from the western Pacific. The return currents in the deeper layer flow through the Indian Ocean to the western Pacific. These features are in qualitative agreement with the structure of the thermohaline circulation shown in Fig. 2a of Gordon (1986).

An issue of interest is the role of the Mediterranean outflow in the formation of the North Atlantic deepwater. It was found in experiment I that the salty and warm water from the Mediterranean Sea sinks to the depth of $1 \sim 2$ km in the immediate neighborhood of the Strait of Gibraltar. A portion of this water spreads westward and becomes the upper deep water of the North Atlantic Ocean. Another portion of the Mediterranean outflow moves northward and upward along an isopycnal surface and outcrops in the Greenland Sea where it joins the water from the Gulf Stream and sinks to form the deep water. This pathway of the Mediterranean outflow is indicated as a tongue of relatively large salinity in Fig. 15, which illustrates the salinity distribution in the meridional cross section at 17°W longitude. In the same figure, the location of the isopycnal surface of 27.1° is indicated by a dashed line as a reference. In short, the Mediterranean outflow plays a significant role in the formation of the North Atlantic deep water in qualitative agreement with observation (Reid 1979).

The salinity cross section is also made for experiment II and is added to Fig. 15 for the sake of comparison.

In this experiment, the Mediterranean water also sinks just outside the Strait of Gibraltar. A portion of this water moves northward. Figure 15b shows a large area of maximum salinity centered around 40°N and extends to 60°N latitude. Since an isopycnal surface remains under the surface halocline and is approximately horizontal in this region, the Mediterranean outflow water moves more or less horizontally and does not outcrop in higher latitudes in contrast to the situation of experiment 1.

c. Budget analysis

To further appreciate the difference in water mass characteristics between the two equilibria, the budgets of heat and water in the oceans are analyzed and described in this subsection.

1) HEAT BUDGET

The latitudinal variations of various surface heat budget components zonally averaged over the Atlantic Ocean are computed from the results of experiment I and illustrated in Fig. 16 as an example. Positive values indicate the heat flux towards the ocean surface and constitutes a heat gain for the surface. On the other hand, the heat flux away from the ocean surface, which constitutes a loss for the surface, is indicated by a negative value. As a whole, the surface of the Atlantic Ocean gains heat from the net incoming solar radiation (NSR) and loses it through net upward long wave radiation (NLR) and the turbulent fluxes of latent (LH)
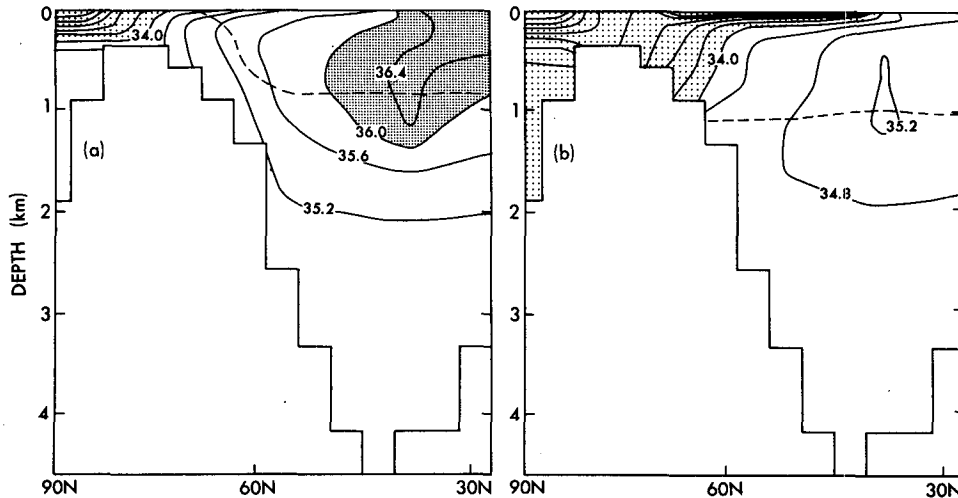
FIG. 15. Latitude–depth section of salinity (ppt) at 17°W longitude in the Atlantic Ocean of the model. Dashed line indicates an isopychnal surface of $\sigma_t = 27.1$. (a) Experiment I, (b) experiment II.

and sensible heat (SH). In addition, an ocean surface loses heat at low latitudes and gains it in high latitudes through oceanic heat flux (OH) which represents a heat supply from the interior to the surface of the ocean. This term is computed indirectly from the following equation obtained from the requirement of surface heat budget:

$$OH = -(NSR - NLR - SH - LH).$$

Figure 17 illustrates the latitudinal distributions of those oceanic heat fluxes which are obtained by zonally averaging the results from the two experiments over the Atlantic Ocean. In the northern North Atlantic, this oceanic heat flux is significantly positive in experiment I, whereas it is rather small in experiment II. As demonstrated below, this difference results from the northward heat transport by the thermohaline circulation in experiment I and the absence of such a circulation in experiment II. In order to examine how

this additional oceanic heat supply in the northern North Atlantic in experiment I is ventilated from the surface, Fig. 18 was constructed. This figure illustrates the latitudinal distributions of the difference in various surface heat budget components between the two experiments zonally averaged over the Atlantic Ocean. According to this figure, the difference in oceanic heat flux is positive over the northern North Atlantic. This positive difference is enhanced by the positive difference in the net incoming solar radiation. On the other hand, all of the differences in the fluxes of latent heat, sensible heat and net upward long wave radiation between the two experiments are negative in the northern North Atlantic. In experiment I, the larger heat supply from the interior to the surface of the northern North Atlantic Ocean is enhanced further by the northward re-
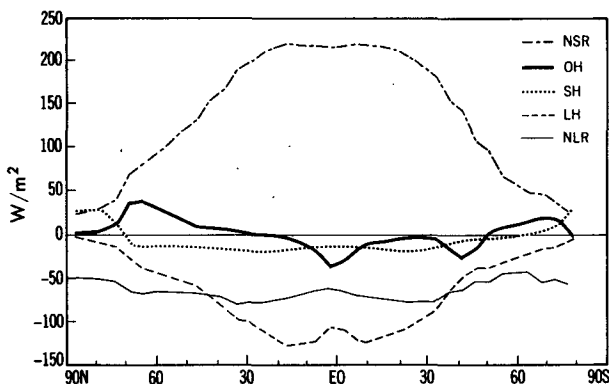

FIG. 16. Latitudinal distributions of various surface heat balance components from experiment I zonally averaged over the Atlantic Ocean. Units are in W m⁻².
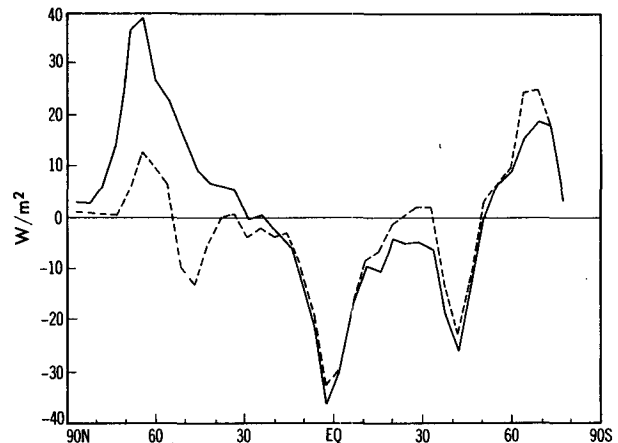

FIG. 17. Latitudinal distributions of oceanic heat flux (OH) zonally averaged over the Atlantic Ocean. Units are in W m⁻². Solid line: experiment I. Dashed line: experiment II.
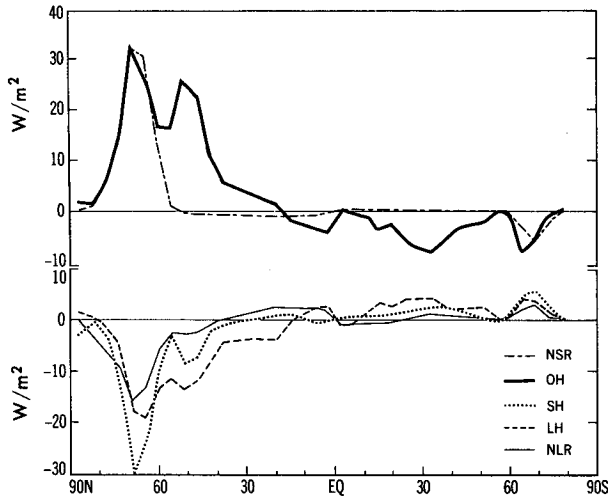
FIG. 18. Latitudinal distributions of the difference in various surface heat balance components zonally averaged over the Atlantic Ocean. Units are W m^{-2}. See explanation of Fig. 17 in text for sign convention.

treat of the margin of sea ice with high surface albedo, whereas the heat supply in the same region is negligible in experiment II. This positive feedback process of sea ice effectively doubles the surface heat gain from the oceanic heat flux and helps maintain higher sea surface temperature over the northern North Atlantic in experiment I despite the enhanced ventilation (or thermal damping) of ocean surface through sensible and latent heat fluxes and long wave radiation.

The difference in oceanic heat flux between the two experiments stems mainly from the difference in the northward heat transport by ocean currents. The northward transport of heat by ocean currents may be subdivided into three components as follows:

$$C \int^A \left(\int_{z_B}^0 vT\rho dz \right) dx = C \int^A \left(\int_{z_B}^0 [v][T]\rho dz \right) dx$$

$$+ C \int^A \left(\int_{z_B}^0 v'T'\rho dz \right) dx$$

$$+ \text{(subgrid scale diffusion)},$$

where C is the heat capacity of sea water; T and ρ denote temperature and density of sea water, respectively; v is the meridional component of ocean current; square brackets indicate the zonal average; and a prime denotes deviation from it; and

$$\int_{z_B}^0 (\quad)\rho dz$$

and

$$\int^A (\quad)dx$$

are the vertical mass integral over the entire depth of ocean and the zonal integral over the Atlantic Ocean,

respectively. The first and second terms in the right-hand side represent the northward heat transports due to meridional overturning and horizontal gyre circulation, respectively, and the third term denotes the northward transport by subgrid scale diffusion. Figure 19 indicates the latitudinal profiles of these three components. Because of the stronger meridional circulation, the overturning component of heat transport in experiment I is much larger than the corresponding transport in experiment II. Although there exists a small difference in gyre transport between the two experiments around 30°N, the difference is trivial. These results indicate that, in experiment I, the northward heat transport by meridional overturning helps maintain the sea surface temperature of the northern North Atlantic higher than experiment II despite strong thermal damping due to the surface fluxes of sensible and latent heat and terrestrial radiation.

2) WATER BUDGET

The components of the water budget at the ocean surface consists of the water supply from precipitation and runoff and water loss due to evaporation. Figure 20 illustrates the latitudinal distributions of the water budget for the Atlantic Ocean. Solid and dashed lines indicate results from experiments I and II, respectively. Owing to higher sea surface temperature, the evaporative loss of water over the North Atlantic Ocean is systematically larger in experiment I particularly in
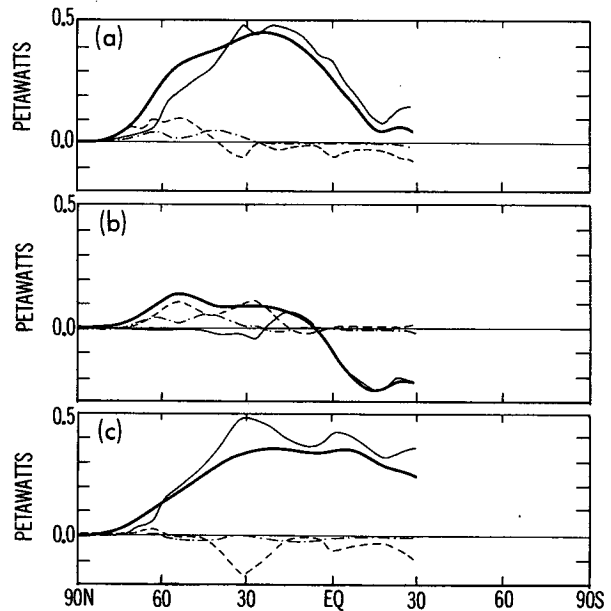

FIG. 19. Latitudinal distributions of various components of northward heat transport by ocean currents in the Atlantic Ocean of the model. Units are in Petawatts. Thick solid line: total transport. Thin solid line: meridional overturning. Dashed line: gyre circulation. Dashed-dotted line: subgrid-scale mixing. (a) Experiment I. (b) Experiment II. (c) Difference between experiments I and II.
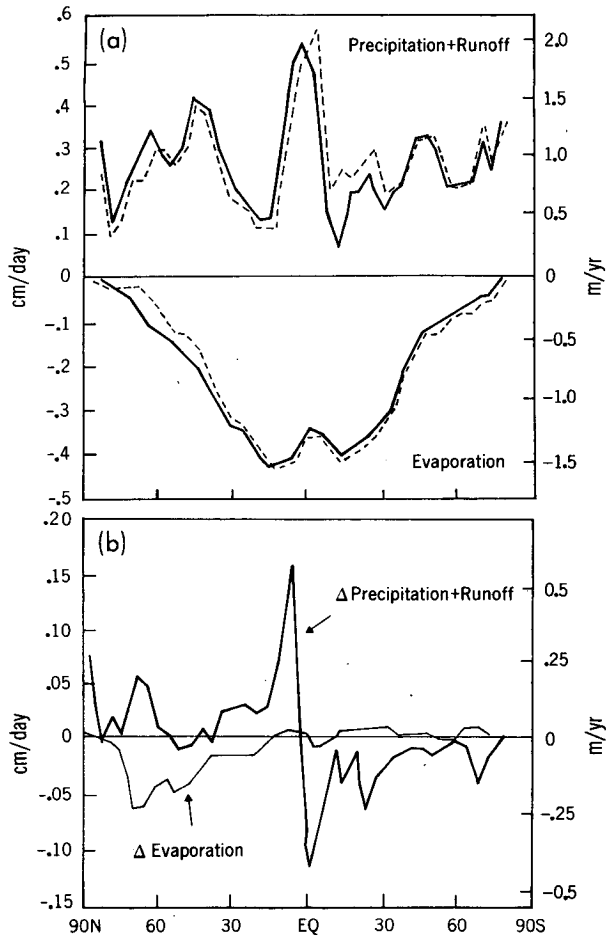
FIG. 20. (a) Latitudinal distributions of surface water balance components (positive contribution; sum of precipitation and runoff. Negative contribution; evaporation) zonally averaged over the Atlantic Ocean. Solid line: experiment I. Dashed line: experiment II. (b) Latitudinal distribution of the difference in the surface water balance components between experiments I and II zonally averaged over the Atlantic Ocean. Thick solid line: difference in the sum of precipitation and runoff. Thin solid line: difference in (− evaporation). Units are in centimeters per day (left) and meters per year (right).

high latitudes. This difference in evaporation rate, in turn, affects both precipitation over the Atlantic and runoff from the surrounding continents. Thus, the water gain from precipitation and runoff in experiment I is also larger than the gain in experiment II in the North Atlantic Ocean. Note, however, that the difference in water gain has more complicated latitudinal structure than the difference in water loss from evaporation. For example, the difference is significantly positive not only in high latitudes but also in low latitudes of the Northern Hemisphere. On the other hand, it is negative in low latitudes of the Southern Hemisphere. This reversal of the sign across the equator is the manifestation of the slight northward shift of the tropical rainbelt which results from the shift of the Hadley cells induced by

the warm surface anomaly of the North Atlantic in experiment I. In addition, the weakening of the indirect Ferrel cell is consistent with the reduction of precipitation rate in the subtropics from experiment II to I. (See the following subsection for the discussion of the difference in the atmospheric meridional circulation between the two experiments.) Averaged over the entire Northern Hemisphere Atlantic, the difference in surface water flux between the two equilibria is only 0.1 Sv due to the compensation between the differences in precipitation and evaporation (see Table A1 in the Appendix). In order to get the general impression of the relative magnitude of the difference in surface water flux, Fig. 21 is constructed. This figure illustrates the latitudinal distributions of zonally averaged, surface water fluxes from both experiments I and II. It clearly shows that the two distributions are very similar to each other and the relative magnitude of the difference between the two is small at most latitudes.

The similarity between the distributions of surface water flux from the two experiments is in sharp contrast to the situation with respect to the surface heat flux discussed earlier. It is well known that an anomaly in sea surface temperature is damped through the heat exchange between the atmosphere and oceans. Over the northern North Atlantic, the ventilation through evaporation and sensible heat flux is much stronger in experiment I with substantially higher sea surface temperature than in experiment II, making the latitudinal profiles of surface heat flux quite different between the two experiments. On the other hand, an anomaly in surface salinity is not reduced systematically by an
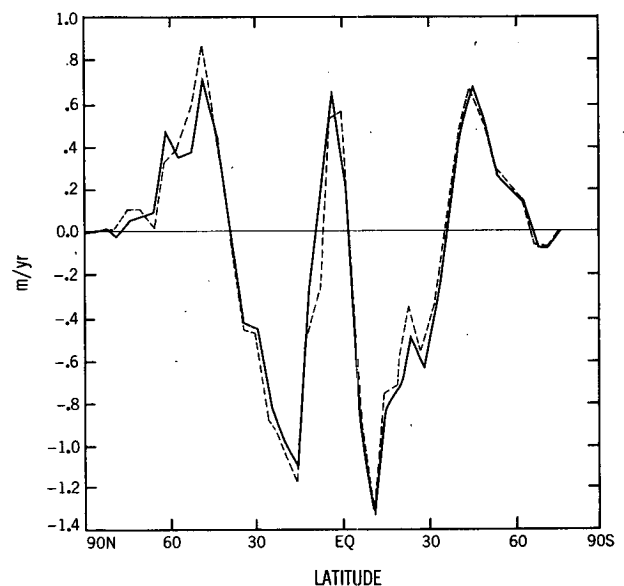

FIG. 21. Latitudinal distributions of net surface water flux (i.e., precipitation plus runoff minus evaporation) zonally averaged over the Atlantic Ocean. Units are in meters per year. Solid line: experiment I. Dashed line: experiment II.
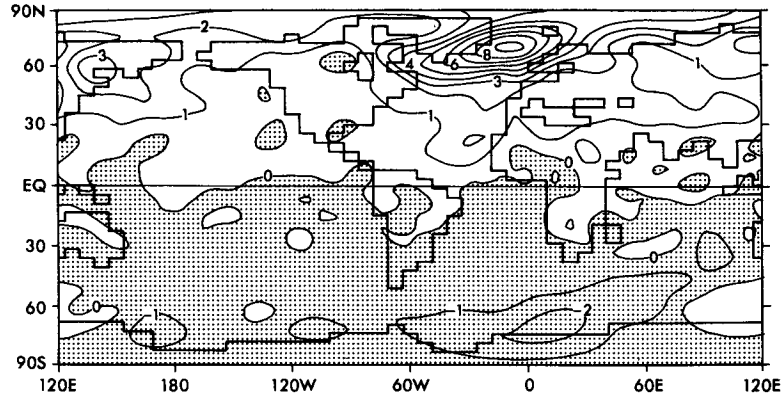
FIG. 22. Difference in surface air temperature (degrees Celsius)
between experiments I and II.

anomaly in surface water flux. In other words, the surface salinity does not directly influence either evaporation or precipitation. This is why the latitudinal profile of surface water flux is very similar between the two experiments despite the large difference in surface salinity over the northern North Atlantic Ocean.

The results described above suggest that the large difference in surface salinity over the North Atlantic Ocean between the two experiments is not due to the difference in surface water flux. Instead, it results from the difference in the residence time of surface water. In experiment I with the thermohaline overturning, the surface water in the northern North Atlantic is continuously replaced by the saline water from lower latitudes, maintaining relatively high surface salinity there despite the dilution by the surface water flux. On the other hand, in experiment II, a major fraction of surface water flowing northward along the European coast recirculates in the subarctic gyre instead of sinking in the Norwegian Sea and its neighborhood. Thus, the replacement of surface water in the northern North Atlantic is much slower than in experiment I. The long exposure of surface water to the diluting influence of surface water flux is responsible for the very low surface

salinity over the northern North Atlantic in experiment II.

In short, the difference in surface salinity between the two experiments over the northern North Atlantic Ocean is attributable to the difference in the exposure of surface water to the diluting influence of positive surface water supply. The duration of the exposure is essentially controlled by the speed of the conveyor belt of the thermohaline circulation.

d. Atmosphere

The two stable equilibria differs significantly from each other not only in the oceans but also in the atmosphere. In this section, a comparison is made between the two atmospheres obtained from experiments I and II.

The difference in surface air temperature between the two experiments is illustrated in Fig. 22. This distribution is very similar to the distribution of the difference in sea surface temperature between the two experiments shown earlier in Fig. 7c. For example, the difference is positive over most of the Northern Hemisphere and is negative in the Southern Hemisphere. It
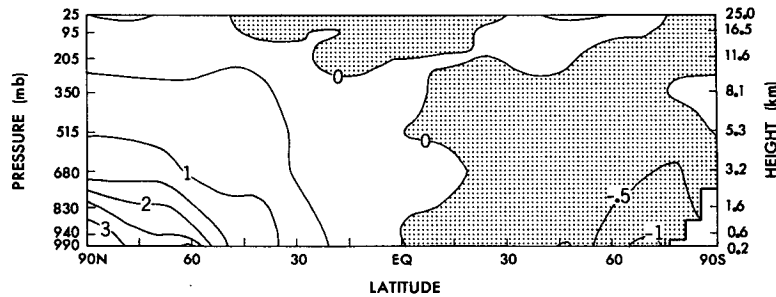
FIG. 23. Latitude–height distribution of the zonal mean difference in atmospheric temperature (degrees Celsius) between experiments I and II. Here, zonal averaging was performed over an entire latitude circle.

is particularly large over the North Atlantic Ocean and
is at a maximum in the latitude belt from 60° to 70°N.
As discussed earlier, the northward advection of surface
temperature by the thermohaline circulation in exper-
iment I and its absence in experiment II accounts for
the positive differences in both sea surface temperature
and surface air temperature in the Northern Hemi-
sphere and negative differences in the Southern Hemi-
sphere over the Atlantic Ocean.

A closer comparison of Figs. 22 and 7c reveals that
the North Atlantic belt of maximum difference in sur-
face air temperature is located about 5° to the north
of the corresponding belt for sea surface temperature.
Since the sea ice coverage in experiment I is signifi-
cantly less than in experiment II poleward of 60°N,
the difference in surface air temperature between the
two experiments is larger than that of sea surface tem-
perature in high latitudes, resulting in the latitudinal
separation of the two maximums mentioned above.

The area of the positive difference in surface air tem-
perature is not confined to the North Atlantic Ocean
and its neighborhood. Instead, it covers the Eurasian
continent and extends all the way to the Pacific Ocean
in the Northern Hemisphere. As previously noted, it
is highly probable that the positive difference in the
North Atlantic Ocean spreads over the entire hemi-
sphere by the zonal advection in the model atmosphere.
The positive difference in the atmosphere, in turn, in-
duces a similar difference in the sea surface temperature
in other oceans of the Northern Hemisphere. Presum-
ably, a similar spread of negative difference occurred
in the Southern Hemisphere.

The large positive difference in the Northern Hemi-
sphere described above is essentially confined to the
lower model troposphere due to the stable stratification.
This is evident in Fig. 23 which illustrates the latitude–
height distribution of zonal mean difference in atmo-
spheric temperature between the two experiments. The
effect of the heating due to the convergence of the
oceanic heat transport into the northern North Atlantic
is further magnified by the positive feedback effect of
sea ice and snow cover, resulting in the polar ampli-
fication of the positive difference in atmospheric tem-
perature between the two experiments. In the Southern
Hemisphere, the difference becomes negative with po-
lar amplification around the Antarctic continent.

Because of this difference in atmospheric tempera-
ture, the meridional temperature gradient and the ver-
tical wind shear in the lower model troposphere over
the North Atlantic Ocean are smaller in experiment I
than experiment II. This difference manifests itself in
the distribution of atmospheric pressures obtained from
these experiments. Figs. 24a and 24b illustrate the hor-
izontal distributions of the 500 mb geopotential height
from experiment I and the map of its difference be-
tween the two experiments. According to Fig. 24b, the
difference is positive in high latitudes whereas it is small
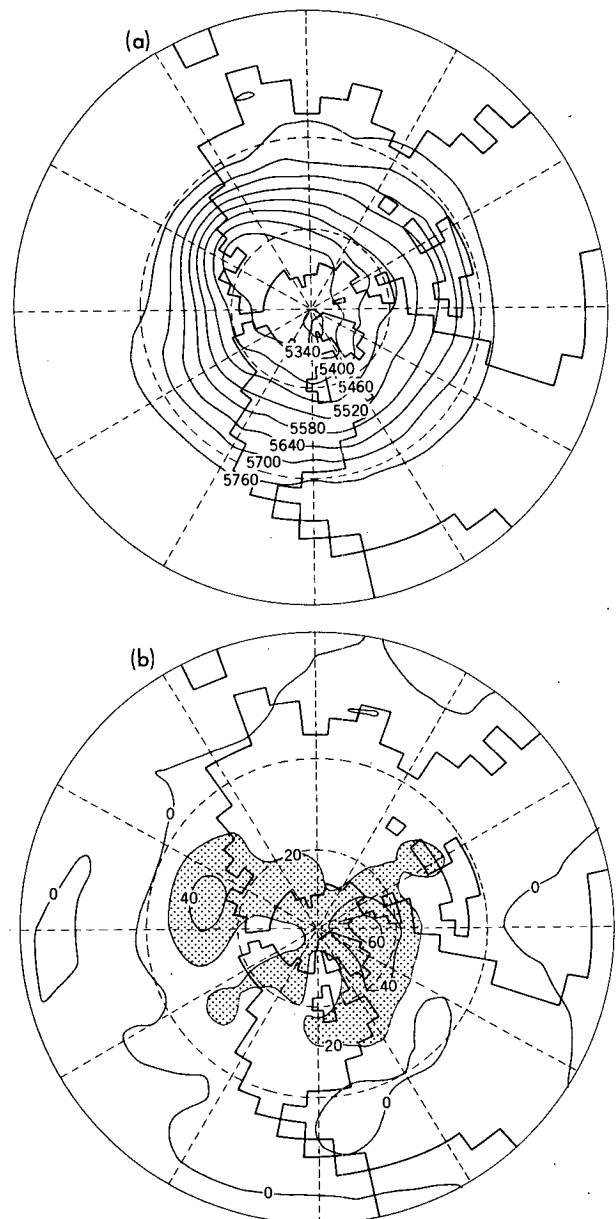and negative in low latitudes. Thus, at the 500 mb

FIG. 24. (a) Geopotential height of 500 mb surface obtained from
experiment I. (b) Difference in 500 mb geopotential height between
experiments I and II (I minus II). Contour intervals: 60 m. Here,
geopotential height represents time mean value over the 3 yr inte-
gration of the atmospheric component of the model.

level, the meridional gradient of geopotential height
and the speed of zonal wind velocity in experiment I
are smaller than those in experiment II.

The maps of sea level pressure from the two exper-
iments and the difference between them are illustrated
in Figs. 25a, 25b and 25c. These figures indicate that
over the North Atlantic Ocean the distributions of sea
level pressure from both experiments are characterized
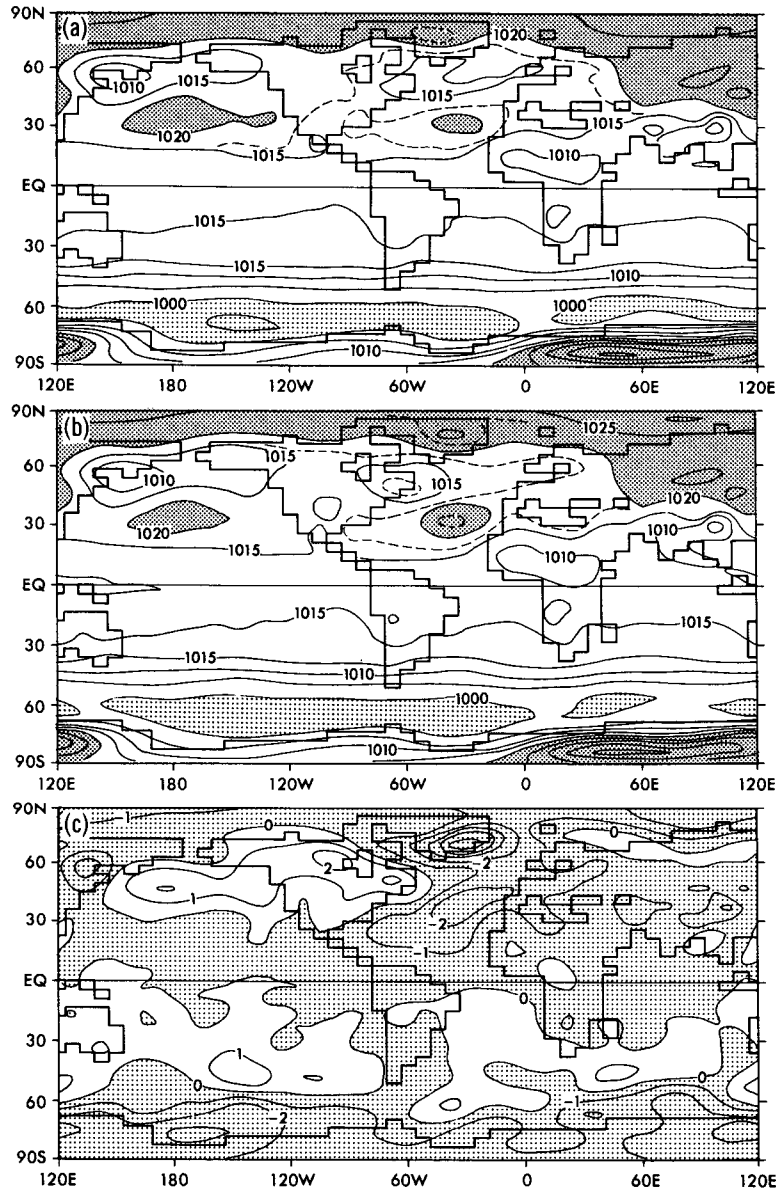by a low over the Labrador Sea and highs over the

FIG. 25. (a) Sea level pressure from experiment I. (b) Sea level pressure from experiment II. (c) Difference in sea level pressure between experiments I and II. Units are in millibars.

Arctic and subtropical oceans. However, as Fig. 25c indicates, the difference in sea level pressure between the two experiments is negative where the Arctic and subtropical highs are located. Thus, the meridional profiles of sea level pressure in experiment I has smaller amplitude than experiment II. It is reasonable to believe this difference in the amplitude of surface pressure pattern is a manifestation of the difference in baroclinicity between the two experiments.

It is reasonable to expect that the difference in atmospheric temperature between the two experiments affects not only the distribution of pressure but also

that of meridional circulation in the model atmosphere. Fig. 26 contains the streamfunction which illustrates the difference in meridional circulation between the two experiments. For reference the streamfunction of meridional circulation itself obtained from experiment I is included in the upper half of this figure. The streamfunction difference in the lower half of this figure indicates an interhemispheric cell with rising motion around 15°N and sinking motion around 15°S latitude. According to Fig. 23, the difference in tropospheric temperature between the two experiments is positive in the Northern Hemisphere and negative in the
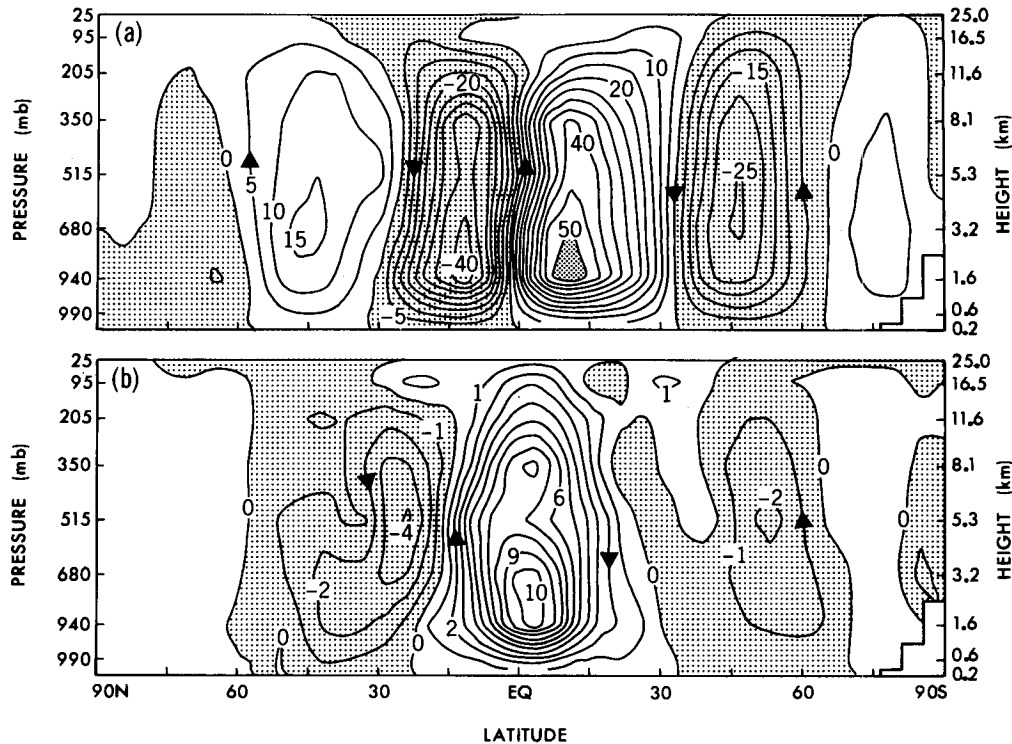
FIG. 26. (a) Streamfunction of meridional circulation in the model atmosphere obtained from experiment I. (b) Streamfunction of the difference in meridional circulation between experiments I and II. Units are in 10^{12} g s^{-1}.

Southern Hemisphere. Thus, this interhemispheric asymmetry of the tropospheric temperature difference maintains the difference in solenoidal field, thereby inducing the meridional cell in low latitudes where the influence of the earth's rotation is relatively small. This interhemispheric cell, in turn, is responsible for making the tropical precipitation in experiment I larger in the Northern Hemisphere and smaller in the Southern Hemisphere than the corresponding precipitation from experiment II as described in the preceding subsection.

Fig. 26 also indicates that, in the Northern Hemisphere, the intensity of the Ferrel cell is weaker in experiment I than II. The reverse holds in the Southern Hemisphere. It is likely that the differences in meridional temperature gradient and baroclinicity between the two experiments are responsible for the difference in the intensities of the Ferrel cells described above. As noted earlier, the meridional temperature gradient in the model atmosphere is larger in experiment I than in experiment II in the Northern Hemisphere, whereas the reverse is the case in the Southern Hemisphere.

The difference in tropical meridional circulation described above is consistent with the difference in precipitation rate between the two experiments. According to Fig. 27 which illustrates the geographical distribution of the difference in precipitation rate over the Atlantic sector of the model, the precipitation rate in experiment

I is larger than in experiment II to the north of the equator and is less to the south. These differences are the manifestation of the slight northward shift of the tropical rainbelt from experiment II to I implied by Fig. 20a. They are consistent with the interhemispheric cell in Fig. 26b illustrating the difference in meridional circulation between the two experiments. The precipitation rate from experiment I is also larger than experiment II over the eastern two-thirds of the North Atlantic in middle latitudes, and the southeastern portion of Greenland and Europe. It is reasonable that these regions of positive difference in precipitation rate approximately coincide with those regions where the difference in sea level pressure shown in Fig. 25c is negative.

Because of these differences, the sum of precipitation and runoff, entering the North Atlantic is larger in experiment I than II. This positive difference, however, is compensated by the difference in evaporation. Thus, the area-averaged water supply at the surface of the North Atlantic differs little between the two experiments as indicated by Table A1 and discussed in subsection 4c.

5. Paleoclimatic implications

The double equilibria described in subsection 4d may have paleoclimatic implications. Broecker et al.
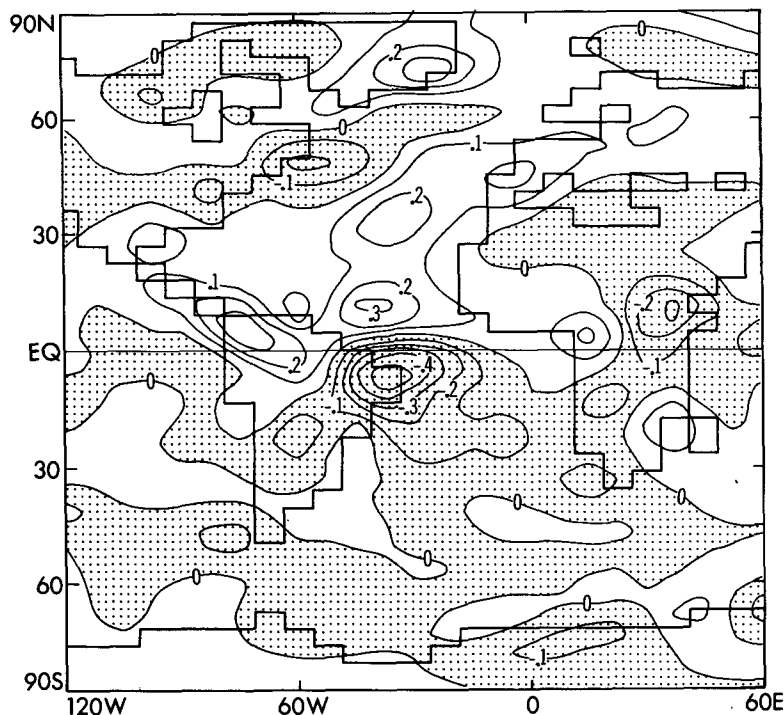
FIG. 27. Geographical distribution of the difference in precipitation rate between experiment I and II. Units are in centimeters per day.

(1985) described the abrupt transition from the relatively warm climate of the Alleröd to the glacial climate of the Younger Dryas around 11 K yr. B.P. (i.e., 11 000 years before the present). They suggested that these two climates are the manifestation of the fact that the ocean–atmosphere system has more than one stable mode of operation. It is tempting to speculate that the two stable equilibria obtained from the present study resembles the climates of the Alleröd and Younger Dryas.

In order to explore this possibility, Fig. 22 which illustrates the difference in surface air temperature between the two experiments, is compared with Fig. 28 from Broecker et al. (1985) containing various paleo-climatic indicators of the Alleröd and Younger Dryas. According to Fig. 22, the area of positive difference in surface air temperature between experiments I and II extends from the North Atlantic Ocean to western Europe and Greenland and covers the northeastern tip of the North American Continent, i.e., Newfoundland. Examining Fig. 28, one notes qualitatively similar difference in surface air temperature between the Alleröd and Younger Dryas Stades. For example, the isotopic analysis of ice cores at the two Greenland stations indicates the surface temperature difference of several degrees centigrade between the two stades. According to the polynological analyses at many continental locations and faunal analyses of deep sea cores, the surface temperature of Alleröd stade was higher than that

of Younger Dryas, not only over the Atlantic Ocean and western Europe but also over the northeastern tip of North America (Broecker et al. 1985). These features are in qualitative agreement with the distribution of the difference in surface air temperature between experiments I and II as described above. It appears, however, that the region of positive difference between the Alleröd and Younger Dryas over western Europe extends further southward than the region of positive difference between the two experiments. This may be reasonable in view of the fact that an extensive ice sheet existed over the North American continent during the transition from Alleröd to Younger Dryas, whereas such an ice sheet is absent in the present experiments.

The comparison between Figs. 22 and 28 indicates that there are many parallels between the climate equilibria obtained from the present experiments and the climates of Alleröd and Younger Dryas, although the former pair has higher North Atlantic temperature than the latter. Furthermore, the chemical analysis of sediment cores by Boyle and Keigwin (1987) suggests that the colder surface temperatures of Younger Dryas in the northern North Atlantic are associated with the reduced flux of northern source water, resembling the oceanic state obtained from experiment II. In view of these evidences, it is reasonable to speculate that the two climates of Alleröd and Younger Dryas are similar to the double equilibria of the coupled ocean–atmosphere system obtained from the present experiments.
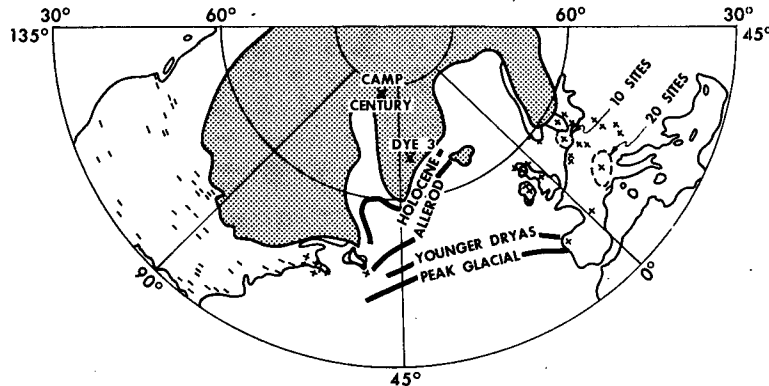
FIG. 28. Map showing the locations of sites at which sediments spanning the 13–9 K yr BP time interval has been studied. At sites designated by a plus, an oscillation in climate corresponding to the Alleröd-Younger Dryas is found. At sites designated by a minus, this oscillation has not been reported. The stippling corresponds to the area covered by ice just before the onset of the Alleröd. The boundaries of icy surface water during the peak glacial, Alleröd, Younger Dryas and Holocene time as reconstructed by Ruddiman and McIntyre (1981) from the analysis of Pachderm shells in deep sea cores are indicated by solid lines (after Broecker et al. 1985).

6. Summary and conclusions

The results from the present numerical experiments suggest that the coupled ocean–atmosphere system may have at least two stable equilibria: one with and another without a thermohaline circulation in the Atlantic Ocean. These two stable equilibria emerge from two time integrations which started from two different initial conditions using an identical model.

In the case with the thermohaline circulation, a portion of the Gulf Stream detaches from the subtropical gyre, flows northeastward and reaches the Norwegian Sea where the water sinks forming the deep water of the North Atlantic. Thus, the surface water over the northern North Atlantic is continuously replaced by warm, saline water from low latitudes where the net surface water flux is negative due to intense evaporation. This helps maintain high surface salinity over the northern North Atlantic despite the dilution in high latitudes where the water gain due to precipitation and runoff exceeds the water loss due to evaporation. In the case without a thermohaline circulation in the Atlantic Ocean, the surface water over the northern North Atlantic is not replaced by the saline water from low latitudes. A major fraction of surface water flowing northward along the European coast recirculates as the subarctic gyre instead of sinking in the Norwegian Sea and its neighborhood. This recirculation prolongs the exposure of northern North Atlantic surface water to the diluting influence of positive surface water flux (i.e., the excess of water gain through precipitation and runoff over the water loss by evaporation), thereby lowering surface salinity. One also notes that a portion of the Labrador current joins the subtropical gyre whereby cold, fresh water flows from the subarctic towards middle and subtropical latitudes. Thus, the surface salinity

and temperature over most of the North Atlantic Ocean are maintained at a level which is substantially lower than the case with thermohaline circulation.

In high latitudes where the sea surface temperature is near the freezing point, the density of surface water depends little upon temperature and is mainly determined by salinity. Thus, the warm, saline surface water of the northern North Atlantic in the former case has a substantially larger density than the cold, fresh water from the latter case. This explains why the surface water of the northern North Atlantic sinks in the former case but does not in the latter case.

Because of higher sea surface temperatures, the evaporation rate over the North Atlantic in the former is larger than the corresponding rate in the latter. However, the water gain from oceanic precipitation and the runoff from the surrounding continents also turned out to be larger over the North Atlantic Ocean and tends to compensate for the difference in evaporation mentioned above. In general, this difference in surface water flux between the two equilibria is much smaller than the surface water flux itself and does not account for the large difference in surface salinity in the northern North Atlantic. Instead, the existence or absence of thermohaline circulation is mainly responsible for the surface salinity difference as discussed in the preceding paragraphs. This is what Reid (1961) suggested in his study of the difference in water mass structure between the Atlantic and Pacific oceans.

Warren (1983) explored the mechanisms which make the surface salinity over the North Pacific significantly lower than that of the North Atlantic Ocean. He attributed the anomalously low surface salinity in the northern North Pacific partly to a low evaporation rate from the relatively cold ocean surface and partly to a small advection of saline surface water from low

latitudes. Gordon and Piola (1983) attributed the relatively salty surface water of the Atlantic Ocean to rapid evaporation as upper-layer water moves northward under the influence of dry atmospheric conditions. However, the results from the present study suggest that the effect of advection alone may be sufficient to explain why the surface salinity of the North Atlantic is much higher than the North Pacific Ocean. As noted in the preceding paragraph, the high evaporation rate over the North Atlantic may be compensated by the high precipitation rate, hardly affecting the net water flux at the ocean surface.

Based upon various geological evidences, Broecker et al. (1985) suggested that an abrupt transition from one climate to another did occur during the Quaternary. The two climates of Alleröd and Younger Dryas stades, as they described, seem to resemble the two stable solutions obtained from the present numerical experiments, although they are somewhat colder than our two stable climates. The resemblance between the two sets of climates suggests that the two equilibria obtained with the model may be physically realizable.

Broecker et al. (1985) and Broecker (1987) also suggested that the thermohaline circulation of the North Atlantic Ocean during the warm period of Alleröd is driven by the extra density of salty surface water which is maintained by the enhanced evaporation from the warmer ocean surface. It should be noted, however, that the difference in the North Atlantic surface salinity between the two equilibria obtained here is attributable to the difference in the residence time of surface water rather than the difference in net surface water flux as discussed in section 4 and the Appendix.

The thermohaline circulations of the North Atlantic Ocean in the two equilibria described here resembles two of the four solutions which were obtained by F. Bryan (1986) from the time-integrations of an ocean model with an idealized sector geography, prescribed sea surface temperature, and prescribed surface water flux. For example, the equilibrium without North Atlantic thermohaline circulation resembles the state which he obtained starting from the initial condition with the symmetric meridional circulation relative to the equator. On the other hand, another equilibrium occurs with the circulation resembling one of two mirror image pole-to-pole circulations which has a sinking branch near the North Pole. Another pole-to-pole cell which sinks near the South Pole may not be realized in the oceans with realistic geography. The equatorward surface Ekman drift currents driven by the intense surface westerlies form a deep meridional cell in the model oceans around the latitudes of the Drake Passage. Such a cell may prevent the development of the pole-to-pole circulation with the Antarctic sinking. Nevertheless, one should not preclude the existence of equilibria other than those obtained in the present study. It is of interest that more than one solution is obtained not only from the simple ocean model, but also from the coupled ocean–atmosphere model with realistic geography.

F. Bryan (1986) has shown that it is possible to induce a transition from one equilibrium to another in his model by imposing a salinity anomaly upon the surface ocean layer in high latitudes. It would be useful to conduct similar experiments by use of our coupled model, thereby determining the nature and magnitude of the forcing which is needed to induce a transition from one equilibrium to another. In view of the result from the present study, one should not eliminate the possibility that the transient (or equilibrium) response of a model climate to a forcing such as the increase of atmospheric carbon dioxide include the shift from one equilibrium state to another (Broecker, 1987). This is one of the topics of current research at the Geophysical Fluid Dynamics Laboratory of NOAA.

In assessing the result from the present study, one should keep in mind that an artificial adjustment of the water exchange at the ocean–atmosphere interface was necessary in order to remove the bias of the model towards the halocline catastrophe. This bias partly results from the tendency of the model to exaggerate the excess of precipitation over evaporation in high latitudes of the Northern Hemisphere. In addition, the absence of seasonal variation in the present model may result in the underestimation of the sinking of salty water. The bias may also stem from the fact that the oceanic component of the model fails to resolve highly localized salinity anomaly and a center of intense sinking in the northern North Atlantic Ocean. Therefore, we plan to construct a coupled ocean–atmosphere model which has seasonal variation, higher computational resolution, and smaller diapychnal subgrid-scale mixing. It is likely that such a model would have a smaller bias and be useful for the reassessment of the double equilibria and its relevance to past climates.

APPENDIX

Water Flux Adjustment

As explained in section 3b, the rate of water exchange at the ocean-atmosphere interface was adjusted in both
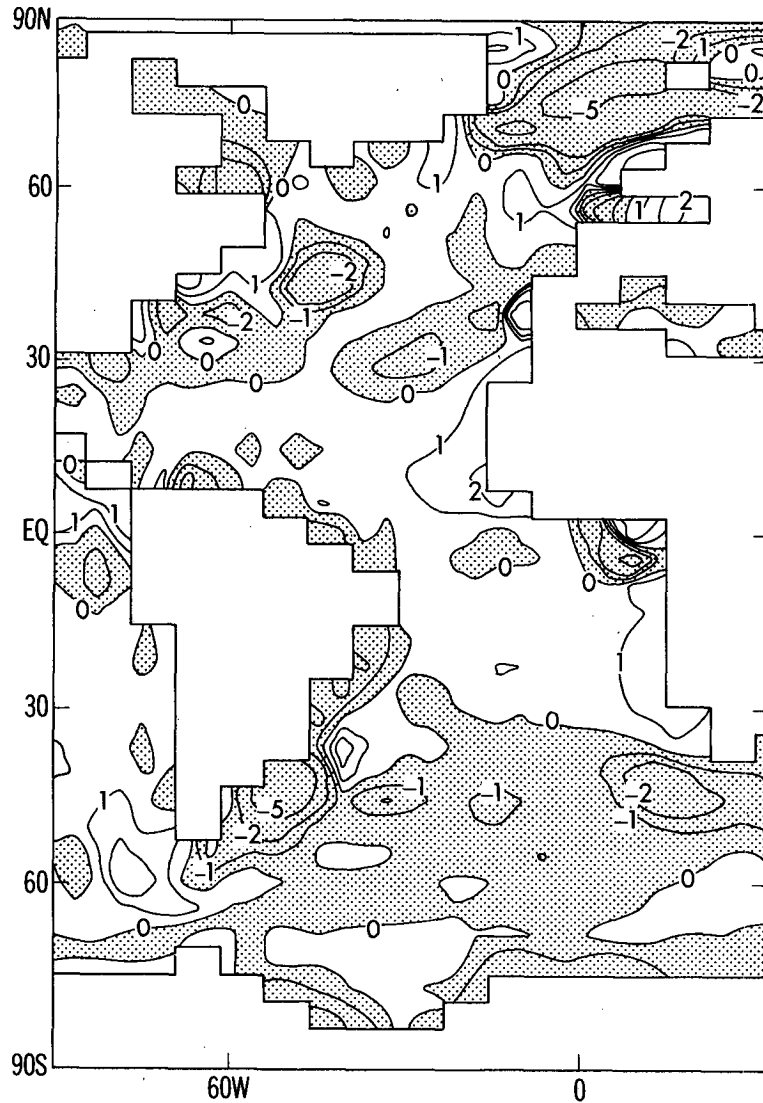
FIG. A1. The map of the adjustment of surface water flux in the Atlantic Ocean.
Units are in meters per year.

experiments I and II. The distribution of this water flux adjustment was determined by the method described in section 3c. Figure A1 illustrates the geographical distribution of the water flux adjustment over the Atlantic sector. The positive or negative values indicate the addition of fresh water or salt, respectively. According to this figure, the water flux adjustment is negative and particularly large over the Greenland–Norwegian Sea. This implies that the model has the tendency to underestimate the surface salinity in this region and requires a large supply of salt there in experiment I in order to maintain the realistic surface salinity and thermohaline circulation in the North Atlantic Ocean. However, in experiment II, which started from the initial condition without the thermohaline circulation in the North Atlantic, even this large salt
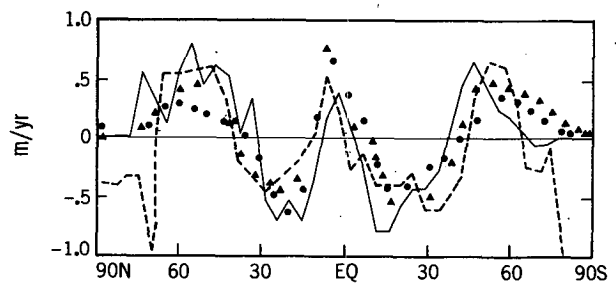
FIG. A2. The latitudinal distributions of zonal mean surface water flux from experiment I. Solid line: surface water flux (i.e., precipitation plus runoff minus evaporation). Dashed line: adjusted surface water flux. The difference between the two water fluxes represents the adjustment of surface water flux. Units are in meters per year. The estimations of actual fluxes are indicated by triangles (Peixóto and Oort 1983) and solid circles (Baumgartner and Reichel 1975).

flux is not sufficient to induce the circulation. Figure A1 also indicates that the field of the water flux adjustment has small-scale patterns and large values near estuaries. This is because the model often misplaces the river mouths and inaccurately reproduces the vertical and horizontal advections of fresh water in and around an estuary.

In order to compare the original and adjusted surface water fluxes with the estimates of the actual water flux, Fig. A2 is constructed. In this figure, the solid and dashed lines illustrate the latitudinal distributions of original and adjusted zonal mean surface water fluxes, respectively. Note that the difference between the two lines indicates the water flux adjustment. In addition, the triangles denote the zonal mean surface water fluxes (i.e., precipitation minus evaporation) estimated by Baumgartner and Reichel (1975) and circular dots show the fluxes deduced from the northward moisture transport estimated by Peixóto and Oort (1983). According to this figure, the estimation of the actual flux is in fair agreement with either the original or adjusted flux. However, in both polar regions, the adjusted flux has extremely large negative values in disagreement with the observed flux which has small positive values there. This result again indicates an extremely large negative water flux adjustment (or large additional salt supply) is required in order to counterbalance the bias of the model towards developing surface halocline and suppressing thermohaline circulation in the North Atlantic Ocean.

The implication of surface water flux adjustment can also be assessed by examining Table A1 which tabulates the water budget of the major ocean basins of the model obtained from the two experiments. The table contains various components of surface water flux area-integrated over each basin and its subdivisions into the Northern and Southern Hemisphere. The surface water flux components shown are the sum of precipitation and runoff ($P + R$), evaporation including sublimation (E), and ($P + R - E$) with and without the adjustment described above. In the bottom of the table, the estimates of the actual water flux components made by Baumgartner and Reichel (1975) are also tabulated for comparison.

This table indicates that, in general, the adjusted values of surface water flux $(P + R - E)_{adj.}$ over the three major basins are more similar to the estimates of the actual flux than the unadjusted values $(P + R - E)$. For example, the area-integrated values of $(P + R - E)_{adj.}$ from experiment I are -0.5 Sv, 0.7 Sv and -0.2 Sv for the entire basins of the Atlantic, Pacific and Indian Oceans, respectively. They are comparable with the values of -0.5 Sv, 0.9 Sv and -0.4 Sv obtained by Baumgartner and Reichel. On the other hand, the corresponding set of unadjusted flux from experiment I are 0.0 Sv, -0.1 Sv and -0.1 Sv and are quite different from the estimates of the actual fluxes. These results suggest that the bias of the present coupled model is attributable to the failure of its atmospheric component to produce realistic surface water flux. However, it is not appropriate to place the entire blame on the atmospheric component in view of the unrealistically large regional water flux required for maintaining the realistic distribution of surface salinity in the northern North Atlantic.

In the Atlantic Ocean of the model, the area-integrated values of $(P + R - E)_{adj.}$ in experiments I and II are -0.5 Sv and -0.5 Sv and are very similar to each other. However, the surface salinity over the Atlantic is quite different between the two experiments. This result clearly indicates that the difference in surface water flux is not a key factor which is responsible for the difference in surface salinity between the two experiments. In short, the existence and absence of thermohaline circulation is mainly responsible for the difference in surface salinity as discussed in section 4c.

TABLE A1. Sum of precipitation and runoff $(P + R)$, evaporation (E), surface water flux $(P + R - E)$ and adjusted surface water flux $(P + R - E)_{adj.}$ area-integrated over the Atlantic including Arctic, Mediterranean Sea, and Pacific and Indian Ocean basins and their Northern and Southern Hemisphere subdivisions. Top and middle section of the table indicates the results from Experiment I and Experiment II and the bottom section contains the estimates of the actual water budget components by Baumgartner and Reichel (1975). Units are Sv = 10^6 m³ s⁻¹.

	Parameter	Atlantic			Pacific			Indian		
		NH	SH	G	NH	SH	G	NH	SH	G
Experiment I	$(P + R)$	1.9	1.2	3.1	3.4	3.0	6.4	0.6	2.2	2.8
	E	1.8	1.3	3.1	3.3	3.3	6.6	0.6	2.2	2.8
	$(P + R - E)$	0.1	−0.1	0.0	0.1	−0.3	−0.2	−0.1	0.0	−0.1
	$(P + R - E)_{adj.}$	0.1	−0.6	−0.5	0.4	0.3	0.7	0.0	0.2	−0.2
Experiment II	$(P + R)$	1.8	1.3	3.1	3.4	3.1	6.5	0.5	2.2	2.7
	E	1.7	1.3	3.0	3.3'	3.3	6.6	0.6	2.2	2.8
	$(P + R - E)$	0.0	0.1	0.1	0.1	−0.2	−0.1	−0.1	0.0	−0.1
	$(P + R - E)_{adj.}$	0.0	−0.5	−0.5	0.3	0.4	0.7	0.0	−0.3	−0.3
Obs	$(P + R)$	2.2	1.2	3.4	4.0	3.6	7.6	0.6	2.2	2.8
	E	2.4	1.5	3.8	3.2	3.5	6.7	0.6	2.6	3.2
	$(P + R - E)$	−0.1	−0.4	−0.5	0.8	0.1	0.9	−0.1	−0.4	−0.5

REFERENCES

Baumgartner, A., and E. Reichel, 1975: The world water balance: Mean annual global continental and maritime precipitation, evaporation and runoff. R. Lee, translator, Elsevier, 1979 pp. + 31 pp. of maps.

Boyle, E., and L. Keigwin, 1987: North Atlantic thermohaline circulation during the past 20,000 years linked to high-latitude surface temperature. *Nature,* 330, 35–40.

Broccoli, A. J., and S. Manabe, 1987: The influence of continental ice, atmospheric CO_2, and land albedo on the climate of the last glacial maximum. *Climate Dynamics,* 1, 87–89.

Broecker, W. S., 1987: Unpleasant surprises in the Greenhouse? *Nature,* 328, 123–126.

——, D. M. Peteet and D. Rind, 1985: Does the ocean-atmosphere system have more than one stable mode of operation? *Nature,* 315, 21–26.

Bryan, F., 1986: High latitude salinity effects and interhemispheric thermohaline circulations. *Nature,* 323(6086), 301–304.

Bryan, K., 1969: Climate and ocean circulation. Part II: The ocean model. *Mon. Wea. Rev.,* 97, 828–829.

——, and L. J. Lewis, 1979: A water mass model of the world oceans. *J. Geophys. Res.,* 84, 2503–2517.

——, 1984: Accelerating the convergence to equilibrium of ocean-climate models. *J. Phys. Oceanogr.,* 14, 666–673.

——, S. Manabe and R. C. Pacanowski, 1975: A global ocean-atmosphere climate model. Part II: The oceanic circulation. *J. Phys. Oceanogr.,* 5, 30–46.

Bryden, H. L., and M. M. Hall, 1980: Heat transport by currents across 25°N latitude in the Atlantic Ocean. *Science,* 207, 884–886.

Gordon, A. L., 1986: Interocean exchange of thermohaline water. *J. Geophys. Res.,* 91(C4), 5037–5046.

——, and A. R. Piola, 1983: Atlantic Ocean upper layer salinity budget. *J. Phys. Oceanogr.,* 13, 1293–1300.

Gordon, C. T., and W. F. Stern, 1982: A description of the GFDL Global spectral model. *Mon. Wea. Rev.,* 110, 625–644.

Levitus, S., 1982: *Climatological Atlas of the World Ocean.* NOAA Professional Pap. 13, National Oceanic and Atmospheric Administration, Rockville, Maryland, 173 pp.

London, J., 1957: A study of atmospheric heat balance, final report. Contract AF(122)-165DDC, College of Engineering, New York University. [NTIS AD117227.]

Manabe, S., 1969: Climate and ocean circulation. Part I: The atmospheric radiation and the hydrology of the earth's surface. *Mon. Wea. Rev.,* 93, 739–774.

——, and K. Bryan, 1969: Climate calculation with a combined ocean-atmosphere model. *J. Atmos. Sci.,* 26, 786–789.

——, J. Smagorinsky and R. F. Strickler, 1965: Similated climatology of a general circulation model with hydrologic cycle. *Mon. Wea. Rev.,* 93, 769–798.

Oeschger, H., J. Beer, U. Siegenthaler, B. Stauffer, W. Dansgaard and C. C. Langway, 1984: Late-glacial climate history from ice cores. J. E. Hansen and T. T. Takahashi (eds.) AGU Monogr. Ser. 29 (M. Ewing Symp. 4) 299–306.

Peixóto, J., and A. H. Oort, 1983: The atmospheric branch of the hydrologic cycle and climate. In: Street-Perrott et al. (eds.). Variation in the Global Water Budget. Reidel, Dordrecht, 5–65.

Posey, J. W., and P. F. Clapp, 1964: Global distribution of normal surface albedo. *Geofis. Int.,* 4, 33–48.

Reid, J. L., Jr., 1961: On the temperature, salinity and density differences between the Atlantic and Pacific Oceans in the upper kilometer. *Deep-Sea Res.,* 7, 265–275.

——, 1979: On the contribution of the Mediterranean Sea outflow to the Norwegian-Greenland Sea. *Deep-Sea. Res.,* 26A, 1199–1223.

Rooth, C., 1982: Hydrology and ocean circulation. *Prog. Oceanogr.,* 11, 131–149.

Ruddiman, W. F., and A. McIntyre, 1981: The north Atlantic Ocean during the last glaciation. *Paleogeogr. Paleoclimatol. Palaeoecol.,* 35, 145–214.

Sasamori, T., J. London and D. V. Hoyt, 1972: Radiation budget of the Southern Hemisphere. *Meterological Monograph,* 13, No. 35, 9–22. in Meteorology of Southern Hemisphere (C. W. Newton Ed.) American Meteorological Society.

Stomel, H., 1961: Thermohaline convection with two stable regimes of flow. *Tellus,* 13, 224–230.

Warren, B. A., 1983: Why is no deep water formed in the North Pacific? *J. Mar. Res.,* 41, 327–347.